# Microstructural and Mechanical Evaluation of Direct Energy Deposited (DED) Titanium-6Aluminum-4Vanadium (Ti-6Al-4V) for repair applications

Department of Mining and Materials Engineering
McGill University
Montreal, Quebec, Canada
April 2018

A thesis submitted to McGill University in partial fulfillment of the requirements of the degree of Master of Engineering in the Department of Mining and Materials Engineering

© Fanny Chainiau, 2018

## Abstract

Direct Energy Deposition (DED) is an Additive Manufacturing (AM) technology allowing the production of near net shape components by depositing layers of laser melted powder or wire. DED is of growing interest to produce and repair components for costly materials such as titanium alloys for the aerospace industry. Titanium alloys are used in the aerospace industry, for their exceptional balance of strength, ductility, fatigue and fracture properties. Among the variety of titanium alloys, Ti-6Al-4V is the most commonly used. However, in addition to the high cost of the raw material, Ti-6Al-4V can lead to important financial expenditures during the maintenance and traditional repair procedures for such parts. The repairing approach is interesting for aerospace Ti-6Al-4V components as the main purpose is to restore or to extend the use of the repaired work piece beyond its normal service life as their replacement component is very expensive. The objective of this work is to explore the microstructure and mechanical properties of AM produced Ti-6Al-4V in a repair context. Characterization campaigns led to the evaluation of the microstructure, hardness, tensile behavior and fatigue crack growth resistance of the AM Ti-6Al-4V added metal, along with a microstructural and hardness analysis of the repaired interface. It was found that the typical microstructure developed during DED deposition induces anisotropy within the part. In terms of mechanical properties, the fabricated parts meet the AMS 4999A standard requirement for hardness and tensile behavior. First investigation in the repair interface suggests that the deposition induce a mechanical weakness within the repaired component.

## Résumé

La Déposition par Energie Directe (DED) est une technologie de fabrication additive (FA) permettant la fabrication des pièces de haute précision dimensionnelle en déposant des couches de poudre ou fil métallique fusionné par laser. La DED a un intérêt grandissant pour l'industrie aérospatiale en termes de production et réparation de matériaux dispendieux tels que les alliages de titane. Ces alliages sont utilisés dans l'industrie aérospatiale pour leur exceptionnel équilibre de résistance, ductilité, et propriétés de fatigue et rupture. Parmi la large variété d'alliages de titane, Ti-6Al-4V est le plus répandu. Cependant, outre le coût dispendieux du matériau brut, l'utilisation du Ti-6Al-4V induit d'importantes dépenses lors de la maintenance et réparation traditionnelle. L'idée de réparer des composants aérospatiaux en Ti-6Al-4V est intéressante pour étendre l'utilisation de la pièce réparée au-delà de sa durée usuelle d'utilisation puisque son remplacement est dispendieux. L'objectif de cette étude est d'explorer la microstructure et les propriétés mécaniques du Ti-6Al-4V produit par FA dans un contexte de réparation. Des campagnes de caractérisations ont été menées pour évaluer la microstructure, la dureté, le comportement en tension et la résistance à la propagation de fissures du Ti-6Al-4V fusionné, accompagnées d'une analyse microstructurale et de dureté de l'interface de réparation. Il a été trouvé que la microstructure typiquement développée lors de la DED induit de l'anisotropie dans le matériau. En termes de propriétés mécaniques, le Ti-6Al-4V produit pas DED respecte les spécifications de la norme AMS 4999A pour la dureté et le comportement en tension. Les premières investigations menées sur l'interface de réparation suggèrent que la déposition provoque une fragilité mécanique au sein du composant réparé.

## Acknowledgements

First, I would like to thank my supervisor, Mathieu Brochu, for giving me the opportunity to work on such an exciting project. Working under your supervision was an incredible experience. Your continued guidance helped me growing into a better person and your valuable insight in my research made me improve as an engineer.

I would also like to thank everyone from the $P^2[AM]^2$ research group for providing me such a friendly welcome in McGill and support throughout my master's studies. I would like to thank Yaoyao Ding and Nejib Chekir for their precious help on this project. I would also like to thank Oscar Sanchez Mata, Mingyang Chen and Flavio Peter Weinstein Silva for being such great friends despite the long night spent working on courses' projects.

I would like to thank all the amazing people I met in McGill and helped me turn Montréal into home. Special thanks must be addressed to Christina Katsari for all the necessary study breaks and to Karan Narang for the great discussions over lunch. It has been a pleasure to get to know Giulia Reita who turned out to be a perfect friend during her short time in McGill. I also want to thank Anas Foul, Laura Sab Leblanc, Konstantinos Korgiopoulos, Maryam Golozar and Konstandina Chalastara for being such great and supportive friends.

I want to express my endless gratitude from my friends and family from home for their constant support. I would like to thank my parents, Alain and Véronique Chainiau for their unconditional love and pride in my accomplishments, as I could not have done so much without their support. I would also like to thank my brother and sister for always being there for me. I would like to thank Cyril Mourissargues for his every day support, and to express special gratitude to Camille Barizien for her indefectible love and support, even from the other end of the word, and for always being here for me, no matter what.

## Contributions of autors

This thesis is based on a manuscript: *Microstructure and Fatigue crack growth of Direct Energy Deposited Ti-6Al-4V*. The candidate is the primary author of this manuscript, which is co-authored by Dr. Yaoyao Ding who provided technical and scientific expertise and Professor Mathieu Brochu in his capacity of research supervisor.

# Table of contents

## List of figures

# List of Tables

# Chapitre 1 - Introduction

## 1.1 Motivation

Additive Manufacturing (usually referred to as AM) is an emerging manufacturing process that was primarily intended for prototyping and is now developed to produce industrial components. According to the ASTM F2792-10 standard [1.1], AM is a “process of joining materials to make objects from 3D model data, usually layer upon layer, as opposed to subtractive manufacturing methodologies, such as traditional machining". The main advantages of AM can be summarized as follow [1.2]: production speed, design freedom, cost saving and green manufacturing. Indeed, AM requires simple steps and does not require the tooling necessary for traditional manufacturing. Thus, complex components can be designed and produced, involving a small amount of raw material waste, which increases the buy-to-fly ratio, fundamental for the aerospace industry [1.3]. It exist seven families of AM, and the most popular ones being Powder Bed Fusion (PBF) and Direct Energy Deposition (DED) [1.4]. DED uses laser welding and robotic principles to produce fully dense part from a powder or wire feedstock and can be used for different materials such as Ni alloys, steels or Ti alloys [1.5] .

Titanium and its alloys are structural materials used in the aerospace industry for weight reduction, high temperature applications, corrosion resistance and space limitation. The most popular of them is Ti-6Al-4V that is used in the aerospace industry for several applications, mainly to make gas turbine engines components [1.6].

During its service life, a component undergoes local impacts, corrosion, variable or regular thermal cycles and stresses, or any harmful use conditions that can create local damage or cracking [1.7.], and increasing the life cycle of components is of major interest for the aerospace industry. Several techniques have been studied to repair cracks and defects and in recent years. The relevance and value of using DED as repair technology is thus increasing. The possibility has been explored for stainless steel [1.7, 1.8] and titanium alloys [1.9] with powder feedstock, leading to the development of building strategies suitable for repair. However, previous studies showed the evolution of the microstructure throughout the repair [1.10] and suggested that it would lead to a reduction of the mechanical performance, still to be validated with more studies.

## 1.2 Objective

The objective of the work presented in this thesis is to provide insight into the characteristics of the DED produced Ti-6Al-4V samples to evaluate the possibility of using the technology to repair aerospace components. The process and the respective parameters have an impact on the performance of the produced part in terms of microstructure and mechanical properties. In addition, the repair creates an interface between the substrate and the build-up where the added material melts the surface of the substrate. Chapter 4 discusses in detail the properties of the build-up part and offers insight into the repair interface between the build-up and the substrate. Characterization campaigns were led to investigate and discuss the microstructure, hardness, tensile behavior and fatigue crack growth resistance.

## 1.3 References


[1] *ASTM F2792-10: Standard Terminology for Additive Manufacturing Technologies*, 2010.

[2] D. Gu, *Laser additive manufacturing of high-performance materials*. Springer, 2015.

[3] H.M. Flower, *High performance materials in aerospace*. Chapman & Hall, 1995.

[4] D. Herzog, V. Seyda, E. Wycisk and C. Emmelmann, "Additive Manufacturing of Metals," *Acta Materialia,* vol. 117, pp. 371-392, 2016.

[5] B. Baufeld, O. Van der Biest and R. Gault, "Additive manufacturing of Ti-6Al-4V components by shaped metal deposition: Microstructure and mechanical properties," *Materials and Design,* vol. 31, pp. 5106-5111, 2010.

[6] C. Leyens and M. Peters, *Titanium and Titanium Alloys, Fundamentals and Applications*. Wiley-VCH, 2003.

[7] A.J. Pinkerton, W. Wang and L. Li, "Component repair using laser direct metal deposition," *Proc. IMechE, Part B: J. Engineering Manufacture,* vol. 222, 2007.

[8] B. Graf, A. Gumenyuk, M. Rethmeier, "Laser metal deposition as repair technology for stainless steel and titanium alloys " *Physics Procedia,* vol. 39, pp. 376-381, 2012.

[9] Nanda Kumar Dey, "Additive Manufacturing laser deposition of Ti-Al-4V for aerospace repair application," Masters, Missouri University of science and Technology, 2014.

[10] E. Brandl, V. Michailov, B. Viehweger and C. Leyens, "Deposition of Ti-6Al-4V using laser and wire, part I: Microstructural properties of single beads," *Surface & Coatings Technology,* vol. 206, pp. 1120-1129, 2011.

# Chapitre 2 - Literature Review

## 2.1 Titanium and its alloys

Titanium is the ninth most plentiful element and the fourth most abundant of the structural metals as its concentration in the Earth's crust is about 0.6%. It has been first discovered in the end of the eighteen's century, but it is considered as a young material since it has only been isolated and developed for the industry from 1910. It is never found in its pure state but can be found in different minerals such as  ilmenite, titanomagnetite, rutile, anatase, and brookite [2.1].

Titanium and its alloys exceptional balance of strength, ductility, fatigue and fracture properties make them suitable for aerospace, biomedical and chemical applications [2.2]. The use of these materials in the aerospace industry is driven by weight reduction, application temperature, corrosion resistance, galvanic compatibility with polymer matrix composites and space limitations. Depending on the application, they can replace aluminum alloys, high strength steels or nickel-based superalloys. Titanium can be found in airfcraft applications such as airframe or gas turbine engines, but also in helicopters and spacecrafts [2.3].

Some characteristics of titanium are shown in Table 2-1 where they are confronted to those of other structural materials, namely iron, nickel and aluminum.

Table 2-1: Characteristics of titanium compared with other structural materials [2.2]

| | Ti | Fe | Ni | Al |
|---|---|---|---|---|
| Melting Temperature (°C) | 1670 | 1538 | 1455 | 660 |
| Allotropic Transformation (°C) | $\beta \xrightarrow{882} \alpha$ | $\gamma \xrightarrow{912} \alpha$ | - | - |
| Crystal Structure | bcc → hex | fcc → bcc | fcc | fcc |
| Room Temperature E (GPa) | 115 | 215 | 200 | 72 |
| Yield Stress Level (MPa) | 1000 | 1000 | 1000 | 500 |
| Density ($g/cm^3$) | 4.5 | 7.9 | 8.9 | 2.7 |
| Comparative Corrosion Resistance | Very High | Low | Medium | High |
| Comparative Reactivity with Oxygen | Very High | Low | Low | High |
| Comparative Price of Metal | Very High | Low | High | Medium |

### 2.1.1 Titanium crystal structure

Titanium is an allotropic material, meaning that it can crystallize in various crystal structures. At room temperature, pure Ti crystallizes into a hexagonal close packed (hcp) structure, called α phase. At higher temperature, above the β-transus (882 ±2°C for pure Ti), the β phase is stable and is a body-centered cubic (bcc) structure. Figure 2-1 shows those structures.

The hexagonal structure being intrinsically anisotropic, variation can be observed in the properties of pure α-titanium, or more generally in the α phase of a Ti alloy. For example, the modulus of elasticity can vary from 100 to 145 GPa depending on the stress axis [2.2].

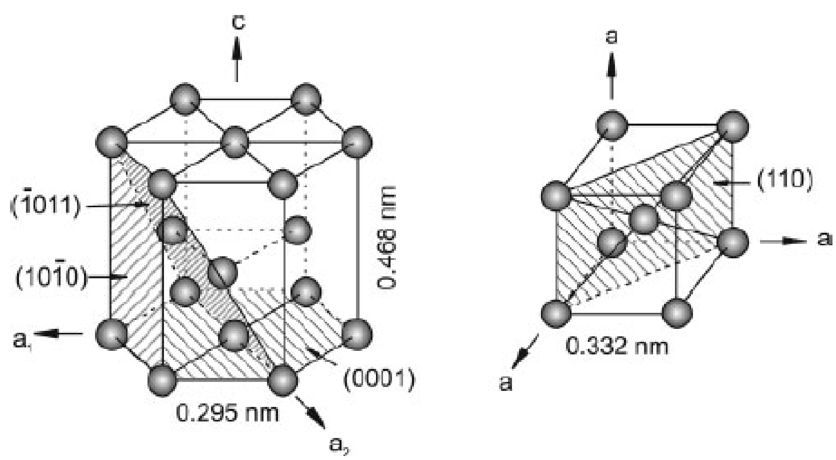


Figure 2-1: Crystal structure of the α and β phases of Titanium[2.1]

Adding alloying elements to Ti allows controlling the crystallization. Additions can either increase or decrease the phase-transformation temperature and are respectively referred as α-stabilizers and β-stabilizers. The single-phase-α and single-phase-β are separated by an α+β phase, which width depends on the solute concentration [2.4].

Depending on the lattice parameters, the properties of the alloys can vary. For example, plastic deformation occurs easier in a body-centered cubic structure than a hexagonal close packed structure.

### 2.1.2 Classification of Titanium alloys

Ti alloys are classified into three categories: "α", "β" and "α + β". Those categories are named after the structural effect of the alloying elements. The effect of those alloying elements in shown on

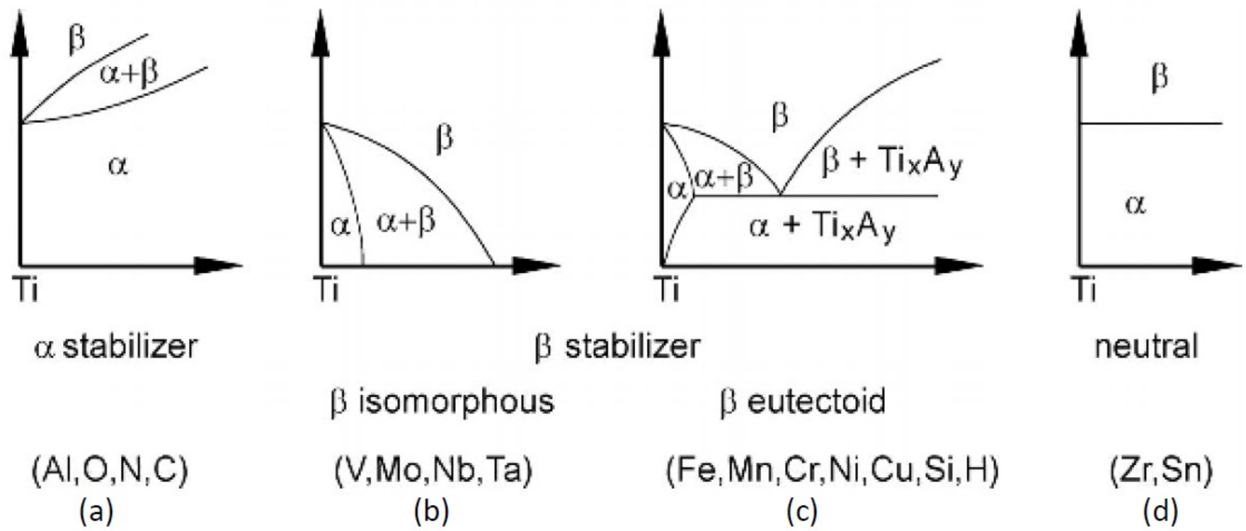


Figure 2-2.

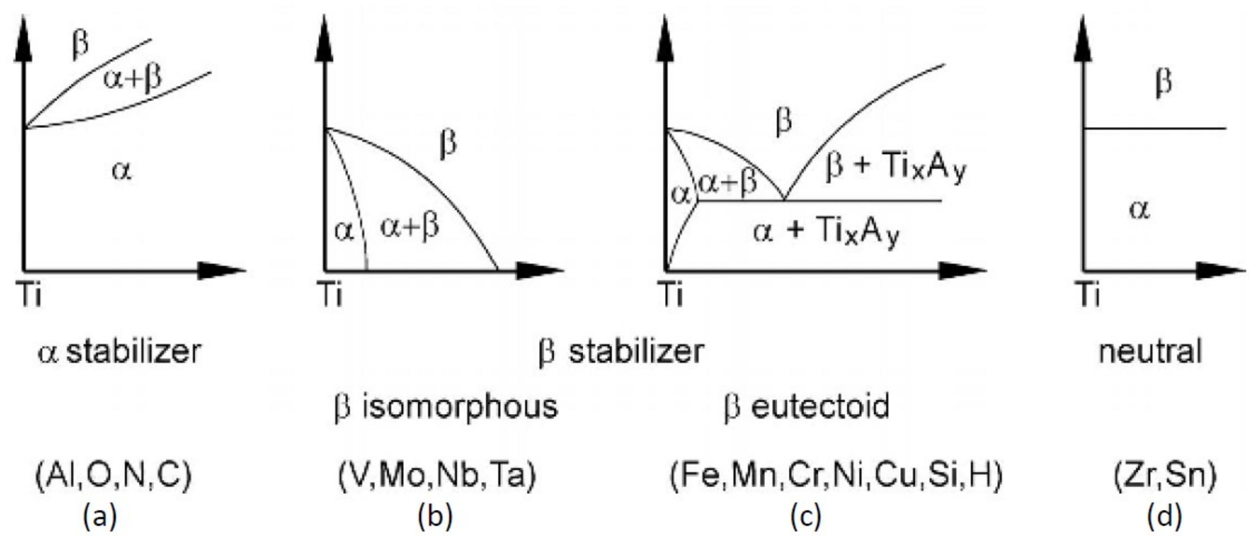


Figure 2-2: Phase diagrams for α stabilizing alloying elements (a), β stabilizing alloying elements (b,c) and neutral alloying elements (d) [2.2]

Alpha alloys contain at least one α stabilizer, namely non-transition elements such as simple metals or interstitial elements [2.4]. The most common α stabilizer is Aluminum, and multicomponent α alloys are classified in term of equivalent aluminum content. According to Rosenberg [2.5], this equivalent content is given by the following equation:

$$[Al]_{eq} = [Al] + \frac{[Zr]}{6} + \frac{[Sn]}{3} + 10[O]$$

According to Wood [2.6], α alloys are characterized by satisfactory strength, toughness, creep resistance, and weldability. They are also suitable for cryogenic applications due to the absence of ductile-brittle transformation of the hcp structure [2.4].

Beta alloys contain at least one β stabilizer, namely transition metals (Molybdenum and Vanadium for example) or noble metals [2.4]. Multicomponent β alloys are classified in term of equivalent molybdenum content. Based on the data from the work of Molchanova [2.7], this equivalent content can be expressed by the following equation:

$$[Mo]_{eq} = [Mo] + \frac{[Ta]}{5} + \frac{[Nb]}{3.6} + \frac{[W]}{2.5} + \frac{[V]}{1.5} + 1.25[Cr] + 1.25[Ni] + 1.7[Mn] + 1.7[Co] + 2.5[Fe]$$

Many commercial beta alloys are available on the market, enough though they only have been considered recently. Those alloys are extremely formable. However, the bcc structure make them prone to ductile-brittle transformation and unsuitable for low-temperature applications [2.4].

The α + β alloys usually contain a mixture of α and β stabilizers and at equilibrium they support a mixture of both α and β phases [2.4]. Those alloys were primarily developed for high strength, high toughness or elevated temperature applications. Among them is the most famous and the most widely used and studied titanium alloy: Ti-6Al-4V [2.8]. The properties and microstructure of α + β alloys can be controlled with heat treatments.

## 2.2 Additive Manufacturing

Additive Manufacturing is to be used in the aerospace industry to produce and repair components. It offers many advantages, such has enabling the fabrication of complex geometries from a CAD file without requiring extra tools, minimizing the finishing procedure by producing near net shape components and significantly reducing the buy-to-fly ratio [2.9]. A recent study [2.10] shows that AM in the aerospace industry represented 2.2 billion USD in 2017 and could reach 20.9 billion USD by 2024.

ASTM International defined Additive Manufacturing as a "process of joining materials to make objects from 3D model data, usually layer upon layer, as opposed to subtractive manufacturing methodologies, such as traditional machining" [2.11] and divided it into seven families: VAT Photopolimerization, Material Jetting, Binder Jetting, Material Extrusion, Powder Bed Fusion, Sheet Lamination and Direct Energy Deposition. Additive Manufacturing is a technique "used to produce solid components by consolidating layers of powder, or wires or ribbons, by partial or full melting. The materials to be deposited are melted by a focused heat source, provided by an electron beam (e-beam), laser beam, or plasma or electric welding arc. Each layer is a 2D section from a final 3D CAD component model: i.e., the 3D geometry of a component is formed by building-up a stack of 2-D profiles, layer-by-layer, by local melting." [2.9]

Gu [2.12] defined the basic procedure for AM processes, which consists of the following steps: creation of a CAD model of the part to be produced, Conversion of the CAD model to STL format, Slicing of the STL file into thin cross-sectional layers, Construction of the part in a layer-by-layer fashion and Postprocessing of the part, including cleaning, surface treatment and heat treatment. Gibson et al. [2.13] divided the procedure into more steps, but they are following the same guideline. Their procedure is shown on Figure 2-3.

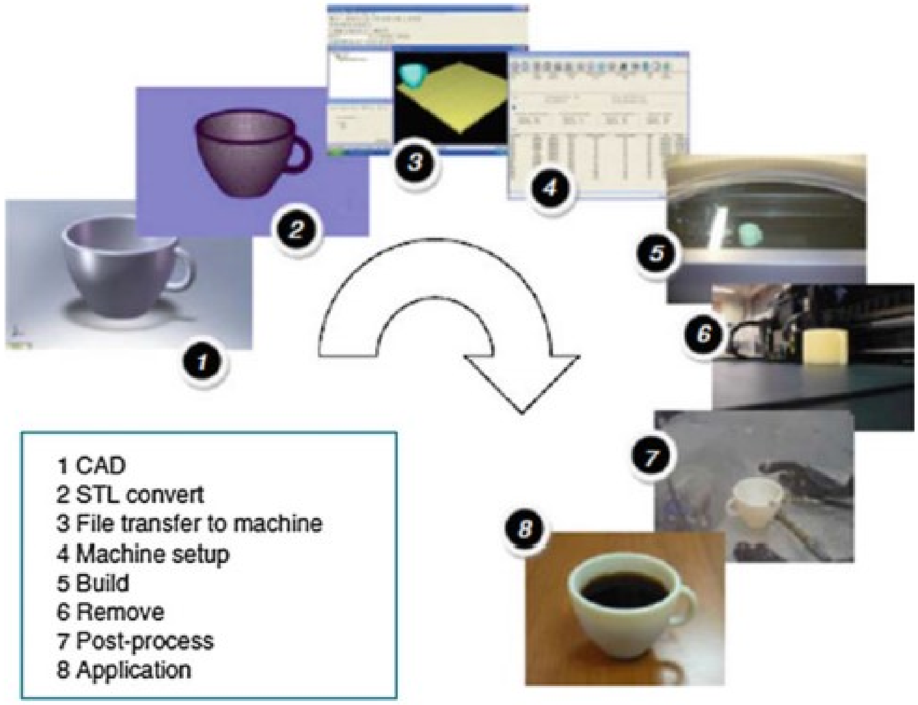


Figure 2-3: Breakdown of the AM process into steps, from the CAD model to the final part [2.13]

AM processes offer numerous advantages compared to conventional manufacturing processes. The major advantages are the following: production speed, reduction in process step and required resources, design freedom, cost saving and green manufacturing. [2.12, 2.13] Indeed, AM processes don't require mold, nor precision positioning for complex machining. It provides with the possible of producing complex components in only one step of manufacturing, plus very few post processing operations, from a CAD model. This can also produce parts that would have to be divided into several parts to be feasible. Finally, the process is environmentally friendly as it uses a nonpollutant source of energy and reduces the waste of raw material. AM also allows the production of near net shape components [2.14].

However, AM technologies induce anisotropy within the part due to the columnar grain growth. This may lead to variations in the mechanical properties of the final component [2.15, 2.16].

Different AM technologies can be used to manufacture Ti alloys and Ti-6Al-4V. We could cite Direct Energy Deposition, Laser Powder Bed Fusion or Electron Beam Melting. For this research, we are going to focus on Direct Energy Deposition (DED).

### 2.2.1 Direct Energy Deposition

DED processes are AM processes "in which focused thermal energy is used to fuse materials by melting as they are being deposited" [2.11] and present numerous advantages for the aerospace industry. For example, they offer the possibility to produce near net shape components, which subsequently reduce the amount of raw material required for the production. They also allow some maintenance, repair and operations (MRO) applications. Those two features can led to important reduction of cost [2.17]. DED processes first used powder but wire was introduced to overcome some issue linked to the use of powder, such as contamination and the cost of high-quality powders [2.18, 2.19]. The different DED processes are Laser Wire Deposition (LWD), Laser Powder Deposition (LPD) and Shaped Metal Deposition (SMD). In this research, we will be focusing on LWD. The deposition system is generally built around the association of a robotic arm, or a moving head and/or platform, with a wire feed system [2.15, 2.20, 2.21, 2.22, 2.23]. A schematic of the DED system is shown on Figure 2-4. The linear heat input is usually in a range of tens to hundreds of J.mm$^{-1}$ for a layer thickness around 0.3–1 mm [2.24].

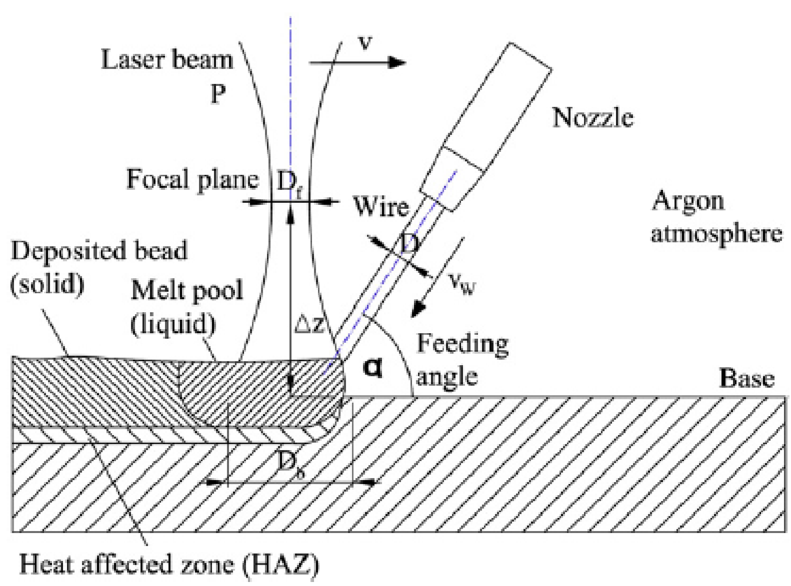


Figure 2-4: Schematic drawing of the wire-feed process [2.20]

The characteristics of the component are highly affected by the parameters of the process. Brandl et al. [2.20, 2.22] established that placing the wire at the leading edge of the melt pool allows to obtain the best performance in terms of surface finish, dimension control and bead quality. To prevent excessive oxidation, all deposits are completed in an argon inert environment.

DED produced parts show very few defects which usually are porosities but Kobryn et al. [2.25] established that porosity are lower than 0.05% per area. Two types of porosity can be observed: lack-of-fusion porosity and gas porosity. The first one is caused by insufficient melting, tends to be irregularly shaped and generally occurs along layer boundaries. The second one is the result of gas entrapment and is characterized by a nearly spherical shape.

### 2.2.2 Effect of deposition parameters on microstructure and mechanical properties

The different deposition parameters such as travel speed, cooling rates, feeding technique will impact the microstructure and mechanical behavior of deposited Ti-6Al-4V. The effects of DED parameters were evaluated in detail by Shamsaei et al. [2.26].

The microstructural characteristics (e.g. morphology and grainsize) of DED parts are strongly sensitive to their thermal history during the build, which may include high heating/cooling rates, significant temperature gradients, bulk temperature rises and more. Since many process variables/parameters impact the thermal history, predicting the microstructural features of DED parts, and the degree of their dependence on process parameters, is still a major challenge. However, overcoming this challenge is vital for establishing the effective control mechanisms for fabricating DED parts with superior mechanical properties. Various authors have investigated the effects of certain parameters on the microstructural characteristics and material properties of DED parts with specific shapes [2.27, 2.28, 2.29]. However, it is still unclear how to apply these findings to fabricate complex parts with various shapes since their microstructures will have a unique dependence on thermal history.

Distinct microstructural regions with fairly different micro-hardness have been reported for stainless steel [2.30], Inconel [2.31] and Ti-6Al-4V [2.32]. This inhomogeneity can be attributed to the time-variable cooling rate of the melt pool and a relatively slower velocity of solidification in the middle region. As a result, higher micro-hardness has generally been measured at the top and bot-tom of DED parts which undergo higher cooling rates during the DED process as compared to the middle region.

Residual stress is defined as the "stress in a body which is at rest and in equilibrium and at uniform temperature in the absence of external and mass forces" [2.33]. The thermal history during the DED process can result in the establishment and evolution of an anisotropic microstructure and the presence of residual stresses throughout the part.

### 2.2.3 DED as a repair technology

During its life, a component is subject to a large variety of loading states and environmental conditions that can induce the apparition of local defects or cracks. Fatigue and stress cracks are common initiators of failures that cause high-performance and high-value components to be discarded as useless [2.34]. That is the case of numerous aerospace components, so studies have been conducted to develop repair techniques and extend components' life cycle. Marazani et al. [2.35] reviewed different technologies that can be used as repair techniques.

Among them, DED has an increasing interest and has been studied for several years. It was first investigated for steel and then extended to other materials like titanium alloys. The technology has a great potential. Graf et al. [2.36] established that metal could be deposited in U- and V-groove shapes in defect-free layers without adjustment. However, the DED processes create an interface between the original component and the added material, made of a Heat Affected Zone, where the component was heated by the added material, and a Fusion Zone, where the added material melted the surface of the component [2.37]. Thus, even if the characteristics of both the component and the build-up part are known, there are still questions about how the interface will behave. Preliminary research from Dey [2.38] expose interesting results on the tensile behavior of the interface.

Graf et al. [2.36] established that thin U-groove shape defects could not be properly repaired. The critical width for repaired as not been established, but they came up with a strategy that produces successful repair. This strategy consists of consecutive layers that are always deposited in the same height difference, adjacent tracks always deposited with the same overlap distance, nozzle tilt for side wall fusion and deposition of material along the side walls first, followed by the middle of the groove. This strategy allows repairing U- and V-groove shapes in Ti-6Al-4V without defects.

### 2.2.4 Additive Manufacturing of titanium alloys

Titanium and its alloys are used in the aerospace industry for specific applications requiring high specific strength even at high temperature and outstanding corrosion behavior [2.1, 2.2]. Ti-6Al-4V is by far the most commonly used and study of all the titanium alloys and commercially pure titanium grades available on the market [2.1]. However, the traditional manufacturing processes to produce Ti-6Al-4V aerospace components involve machining and thus a lot of waste of raw material. This led to the investigation of several potentially lower cost processes [2.17]. The Oak Ridge National Laboratory established that in addition of significantly reducing the buy-to-fly ratio almost to 1:1, Additive Manufacturing (AM) can induce a cost reduction of 50% for the production of aerospace components [2.39].

However, the AM processes have a large impact on the characteristics of titanium alloys as the thermal history in the component strongly influences the crystallographic texture, especially for the Ti-6Al-4V alloy which can develop up to 12 variant microstructures [2.40].

## 2.3 Ti-6Al-4V

Ti-6Al-4V was one of the first titanium alloys to be made. It was developed in the United States in the early 1950s. This alloy is very popular thanks to its good balance of properties, and because it is well known as it is widely developed and tested [2.1].

According to [2.2], this alloy presents an exceptional balance of strength, ductility, fatigue and fracture properties. However, its operating temperature is limited by its low creep performance. Ti-6Al-4V is commonly used for airframe and engine components. The phase diagram of the alloy is given on Figure 2-5.

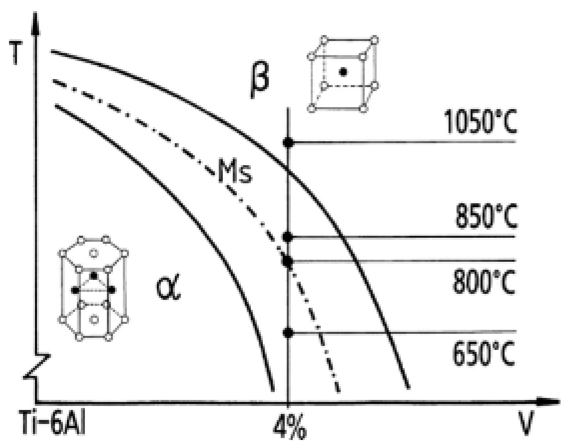


Figure 2-5: Phase diagram of Ti-6Al-4V [2.4]

Usually, the alloy is manufactured through a wrought or cast process. Nonetheless, several researches have been and are still conducted to develop new processes for those alloys, mainly in additive manufacturing. The composition of the wrought alloy is given in Table 2-2. The chemical requirements for the direct deposited alloy are very close, the only difference being that the maximum carbon content is slightly higher (0.10 w%) and some other elements can be found [2.41].

Table 2-2: Chemical composition of wrought Ti-6Al-4V [2.42]

| Element | Composition, % (mass/mass) |
|---|---|
| Nitrogen, max | 0.05 |
| Carbon, max | 0.08 |
| Hydrogen, max[B] | 0.015 |
| Iron, max | 0.30 |
| Oxygen, max | 0.20 |
| Aluminum | 5.5–6.75 |
| Vanadium | 3.5–4.5 |
| Yttrium, max | 0.005 |
| Titanium[C] | balance |

### 2.3.1 Microstructural growth

The growth of the solid within the grain is achieved by addition of atoms from the liquid to the solid itself. The stability of the liquid/solid interface will then affect the microstructure of the deposited metal. The growth can be either planar, cellular or dendritic [2.43]. The three growth methods are shown on Figure 2-6.

Planar growth is characterized by the lack of development of a specific substructure and the growth is perpendicular to the solidification front. Cellular growth lead to the formation of uniformly spaced cells along the growth front. Dendritic growth is primarily controlled by crystallographic considerations and it will occur along specific directions where the growth rate and attachment kinetics are optimized. Dendritic growth can be either columnar when the dendrites form a well-developed substructure or equiaxed in the case of spontaneous nucleation of dendrites.

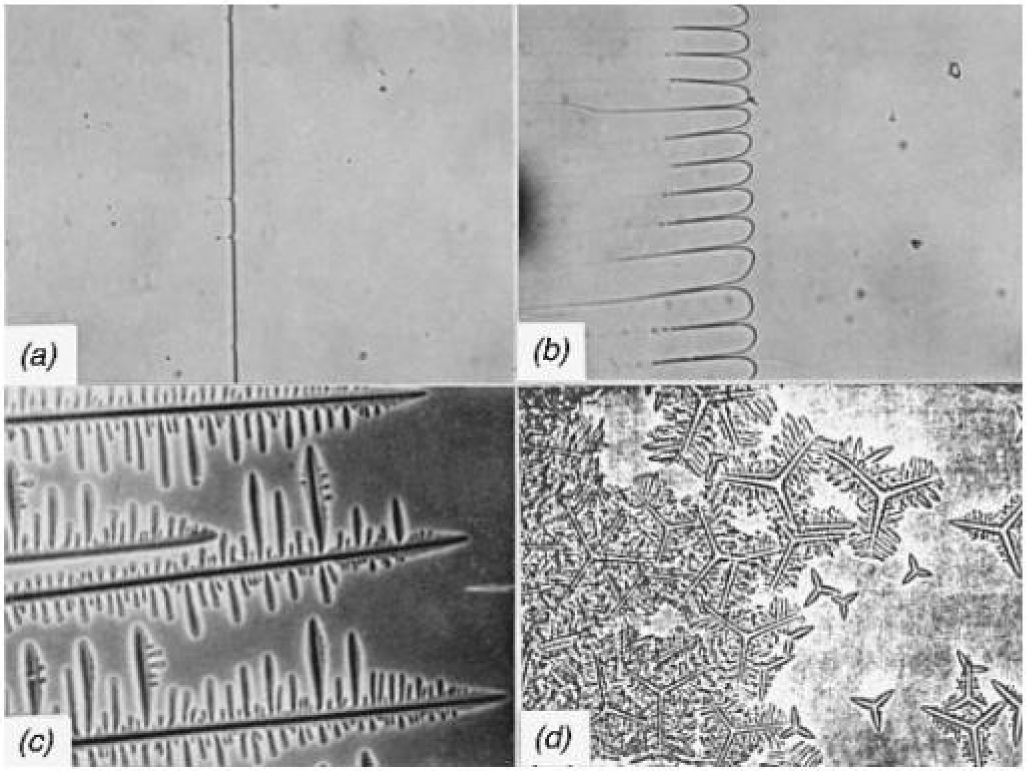

Figure 2-6: Basic solidification modes; a) planar solidification, b) cellular solidification, c) columnar dendritic solidification, d) equiaxed dendritic solidification [2.37]

### 2.3.2 Microstructures of Ti-6Al-4V

The microstructure of Ti-6Al-4V is highly dependent on the process used and the thermal history of the component. For conventional processes, Ti-6Al-4V tends to develop three types of microstructure: lamellar, equiaxed or bimodal.

The lamellar structure results from slow cooling initiated above the β-transus temperature. This leads to nucleation and growth of the α-phase in plate form starting from β-grain boundaries. Different cooling rate can lead to either coarse (plate-like alpha) or fine needle-like structure (acicular alpha) or can even develop Widmanstätten structures. Depending on the initiate temperature, quenching can to finer structure or transformation structures such as martensite. Sargent et al. [2.40] established that the transformation from above the β transus temperature follows a classic Burgers relationship such that the respective closed-packed planes and directions of the parent beta and product alpha phases are parallel to each other. Because of the large variety of those plans and related directions in a bcc crystal, up to 12 distinct alpha variants may be developed.

The deformation procedure induced by extensive mechanical working in the α+β field leads to the breakup of lamellar alpha into equiaxed alpha [2.4]. This microstructure can also be obtained after a recrystallisation anneal followed by slow cooling. Anneal followed by water quenching and aging isolates primary α-grains in a transformed β matrix. This procedure can also form α-precipitates. This bimodal structure is made of α grain in a β matrix with α lamellae between the grains. The different types of microstructure of Ti-6Al-4V are given in Figure 2-7. Other structures can develop in Ti-6AL-4V, mainly in AM parts, which will be discussed later.

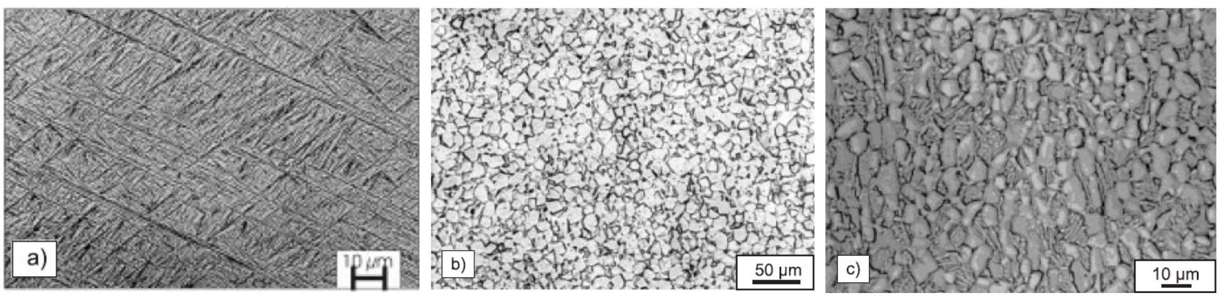


Figure 2-7: Microstructures of Ti-6Al-4V - a) lamellar structure; b) coarse equiaxed structure; c) bimodal structure[2.44]

The microstructure of Additively Manufactured Ti-6Al-4V is different from those of the wrought or cast alloy. Brandl [2.20] described in details the microstructure of a single deposited bead and Baufeld [2.18] focused on multi-layers builds.

Single bead is the smallest unit of Additive Manufacturing. Figure 2-8 shows an etched cross-section of a LWD produced bead where the different microstructural areas are identified. BM is the Base Material, the substrate on which the bead was deposited. This zone shows a bimodal microstructure made of globular primary α-grains in a basket weave α+β matrix. $HAZ_{(\alpha+\beta)}$ is the zone heated to peak temperature below the β transus temperature. In the secondary $HAZ_{(\alpha+\beta)}$, there is a limited change compared to the base material. The lamella width of the basket-weave (α+β) matrix increased slightly and the grain size of the primary α-grains remained approximately constant. In the primary $HAZ_{(\alpha+\beta)}$, the basket-weave structure of the (α+β) matrix seems to change substantially to a colony structure, and the width of the α-lamellae seems to be finer. $HAZ_\beta$ is the zone heated to a peak temperature above the β transus temperature and below the solidus temperature. Here, the primary α-grains decreased in size or dissolved completely, and the prior β-grains increased in size slightly or substantially, depending on the peak temperature reached. CG is the Columnar Grain zone where the material is melted as the peak temperature exceeded the liquidus temperature. This zone is characterized by columnar prior β-grains with basket-weave structure and few martensitic α. Within this zone, we can differentiate the Fusion Zone (FZ) which results from the solidification of the melt pool of the base (for single bead or first deposited layer) or of the previously deposited layers (multi-layers built), and the Added Material (AM).

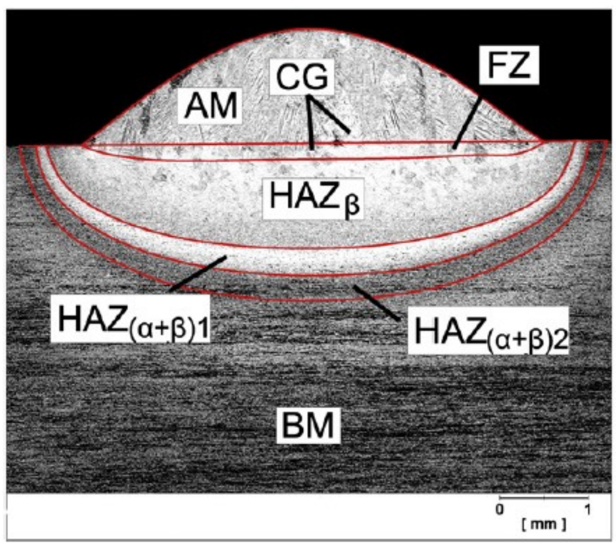


Figure 2-8: Microstructure of the single bead deposited with LWD [2.20]

In multi-layer builds , the columnar prior β grains grow throughout the layers and the microstructure is characterized by Widmanstätten structures made of α phase lamellae in a β phase matrix exhibiting either a basket weave or a colony structure [2.15]. Two regions can be observed, a bottom region with parallel bands and a top region without these bands. Those bands result from thermal history of the process and have been reported for LWD [2.8, 2.18], SMD [2.45, 2.46] and Electron Beam Deposition [2.14]. Columnar grains and layers or shown on Figure 2-9.

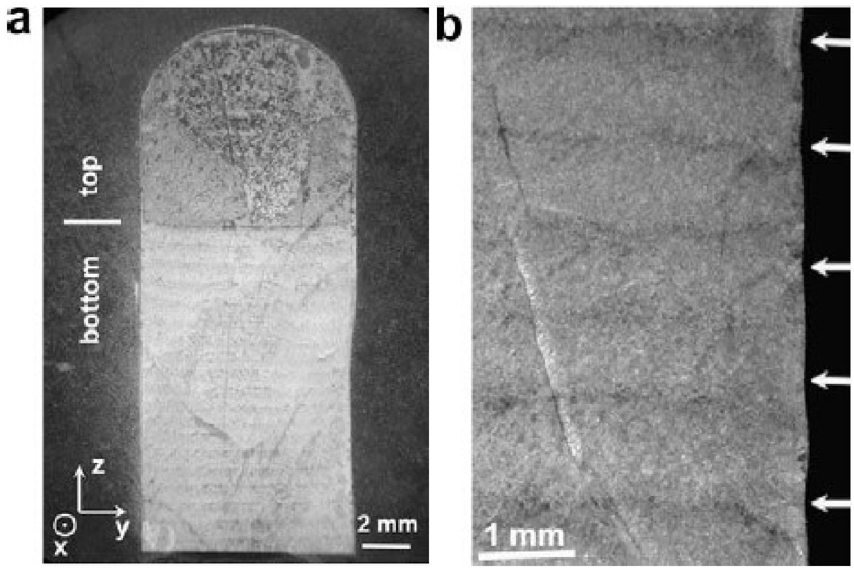


Figure 2-9: a) Etched cross-section of a multi-layer build; b) focus on the parallel bands [2.18]

Columnar grains with a basket-weaved structure is also typically found in plasma deposited Ti-6Al-4V [2.47]. Pulsed-beam builds were characterized by thin a-laths oriented in a Widmanstätten basket-weave pattern [2.48].

### 2.3.3 Defects in DED Ti-6Al-4V

DED processes induce very few defects in the part. However, it is important to notice that porosity can form, and that the thermal history of the process leads to the creation of residual stress.

Two types of porosity can be observed in DED Ti-6Al-4V parts: lack-of-fusion porosity and gas porosity [2.25]. Those porosities are shown on Figure 2-10. Lack-of-fusion porosity result from an insufficient or incomplete melting and are characterized by irregular elongated shapes. Gas porosity are generally spherical and are form by gas entrapment during the deposition [2.49]. Lack-of-fusion porosity are sometimes referred to as interlayer porosity and gas porosity as intralayer porosity [2.25].

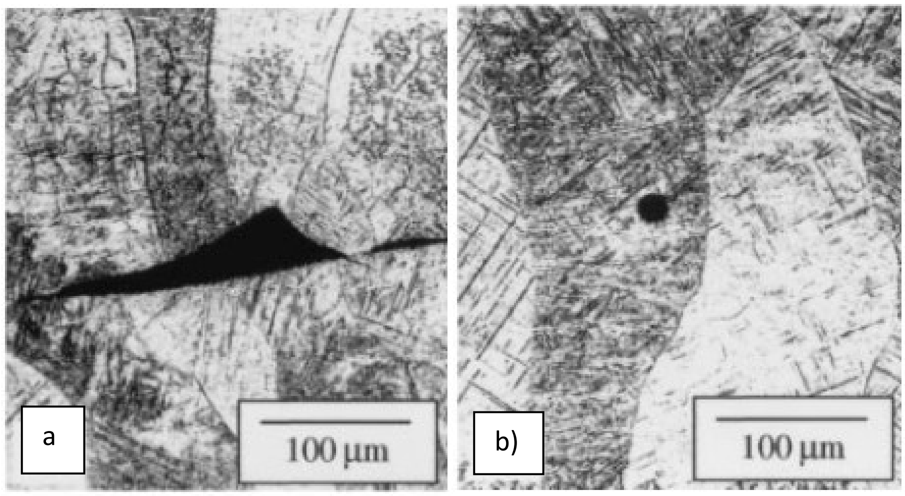


Figure 2-10: Porosities in DED Ti-6Al-4v, a) lack-of-fusion porosity, b) gas porosity [2.25]

Residual stress can be defined as the stress remaining in an object in the absence of external loading [2.50]. In DED Ti-6Al-4V parts, residual stresses remain in the part as a result of an excessive temperature gradient and are detrimental to the stability of the structure [2.51]. In the aerospace industry, residual stresses are very critical as materials operate near their limits. In DED components, thermal stresses induced by the solidification of the previous layers can lead to the creation of distortions within the component that can result in some cases in the fracture of the component [2.52]. Stress-relief heat treatments can be performed to avoid all the issues linked to the presence of residual stresses.

### 2.3.4 Mechanical properties

Most of the studies on AM Ti-6Al-4V reveal that the mechanical properties are as good as or better than conventionally fabricated Ti-6Al-4V in terms of hardness, tensile behavior and fatigue. [2.17] Lewandoski and Seiti [2.53] reviewed the large majority of studies on microstructural and mechanical analysis of AM Ti-6Al-4V. Some of those studies are discussed here.

In the different standards, the mechanical requirements are expressed in terms of tensile properties. Therefore, those requirements for Ti-6Al-4V are gathered in Table 2-3 accordingly to the different standards related to the processes of interest (wrought and cast as a reference for the substrate and DED and PBF for the AM part).

Table 2-3: Tensile requirements for Ti-6Al-4V alloys

| | | UTS | | 0.2% YS | | Elongation | Red. Of Area |
|---|---|---|---|---|---|---|---|
| | | **MPa** | **ksi** | **MPa** | **ksi** | **%** | **%** |
| Wrought [2.42] | | 895 | 130 | 825 | 120 | 10 | 15 |
| Cast [2.54] | | 860 | 125 | 758 | 110 | 8 | 14 |
| DED [2.41] | **X & Y** | 889 | 129 | 799 | 116 | 6 | - |
| | **Z** | 855 | 124 | 765 | 110 | 5 | - |
| PBF [2.55] | **X & Y** | 895 | 130 | 825 | 120 | 10 | 15 |
| | **Z** | 895 | 130 | 825 | 120 | 10 | 15 |

If tensile testing allows characterizing efficiently an alloy, we can also look into a few other properties. The easiest to mention must be the hardness. The reference value for the wrought alloy is around 360 HV [2.4].

Those two criteria, tensile properties and hardness, are studied in the literature from coupons printed using a DED process. Table 2-4 gathers some of those results for DED Ti-6Al-4V.

Table 2-4: Tensile properties of DED Ti-6Al-4V

| | | | UTS MPa | O.2% YS MPa | Elongation % | Modulus GPa | Hardness HV |
|---|---|---|---|---|---|---|---|
| Kobryn [2.56] | ***Powder*** | **X & Y** | 1109 | 1065 | 4.9 | 126 | - |
| | | **Z** | 832 | 832 | 0.8 | 112 | - |
| Mok et al. [2.57] | ***Wire*** | **X & Y** | 958 | 812 | 2 | 123 | 330 |
| | | **Z** | 1011 | 812 | 2 | 123 | |
| Amsterdam [2.58] | ***Powder*** | **X & Y** | 1153 | 1052 | 5.3 | - | - |
| | | **Z** | 1141 | 1045 | 9.2 | - | - |
| Baufeld [2.59] | ***Wire*** | **X** | 956 | 895 | 5.5 | 122 | 351 |
| | | **Z** | 897 | 805 | 7.4 | 121 | 365 |
| Caroll et al. [2.24] | ***Powder*** | **X** | 1041 | 945 | 17.6 | - | 333 |
| | | **Z** | 1063 | 960 | 13.3 | - | |

The fracture mechanism occurring during pure tensile testing is Mode I. This opening results from a tensile stress normal to the plane of the crack [2.60]. Carroll et al. [2.24] suggested that static tensile testing done in the X direction would promote a Mode I type of fracture along the prior β grain boundaries which is in agreement with Baufeld's comments [2.15]. The tensile loading on the grain boundaries is shown on Figure 2-11.

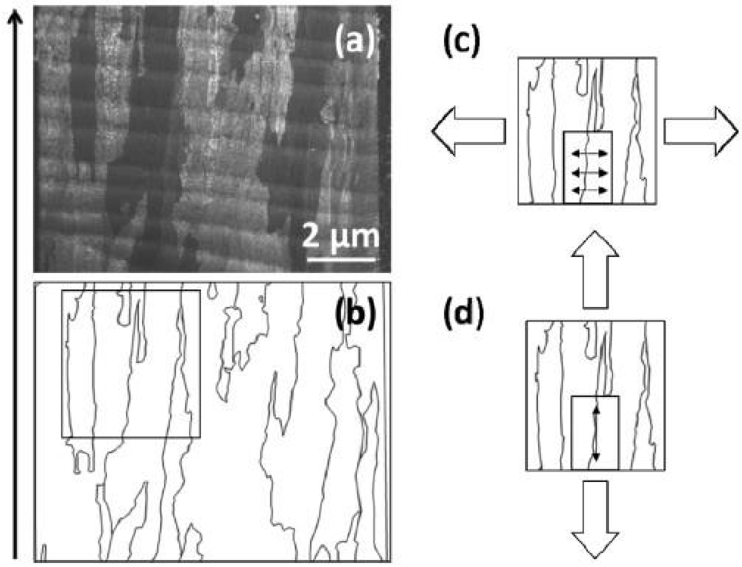


Figure 2-11: a) Optical micrograph showing the β grains; b) Associated outline of the columnar prior β grains; Schematic Mode I opening c) when tested in the X direction and d) when tested in the Z direction [2.24]

The fracture surface of broken Ti-6Al-4V tensile coupons shows dimples, which are the sign of ductile behavior. The shape and distribution of the dimples depend on the fabrication conditions of the alloy but also on the testing parameters. [2.61] Examples of fracture surface are shown on Figure 2-12.

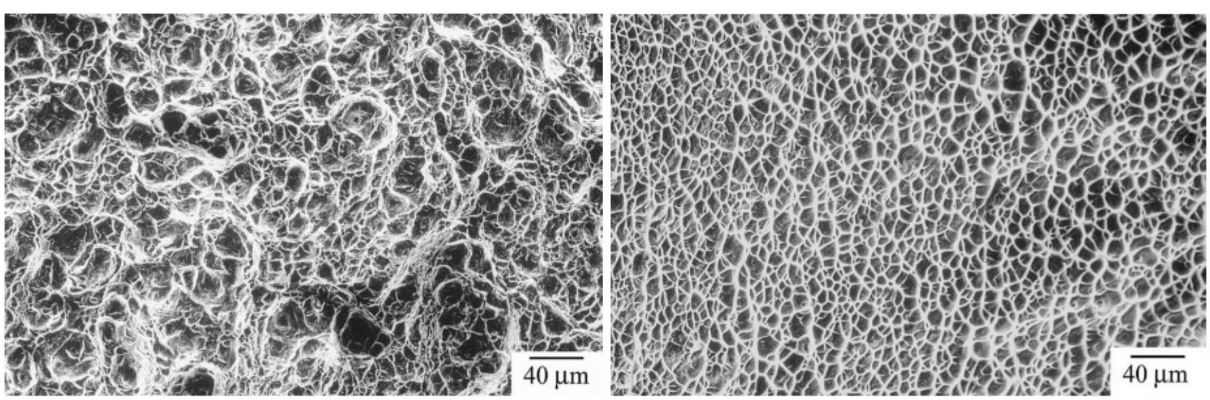


Figure 2-12: SEM pictures of the fracture surface of cast annealed Ti-6Al-4V, a) central region of the coupon, b) near the shear lip [2.61]

Fatigue Crack Growth Rate (FCGR) is mechanical evaluation of the material performed to assess the behavior of crack propagation under repeated cycles. This test allows to determine the fatigue crack growth rate from near-threshold to controlled stability [2.62]. The results of FCGR tests are usually plotted on a curve opposition the stress intensity and the crack growth rate. The typical FCGR behavior of wrought or cast annealed Ti-6Al-4V is shown on Figure 2-13. On this curve, we can distinguish 3 different areas illustrating the evolution of the behavior of the material during the test. First, the near threshold region corresponds to the crack opening. The stress intensity threshold is a material dependent value under which the crack does not propagate. Then, the middle part of the curve illustrates the crack propagation under the Paris' law. The final region at the end of the test corresponds to the instability leading to the fracture. This is governed by the fracture toughness of the material. [2.63]

Fatigue crack growth resistance (FCGR) generally is improved with microstructures containing increased amounts of transformed β morphology, the slowest crack growth rates are frequently observed in products such as castings and β annealed or β processed parts. Age hardening reduces FCGR due to lower intrinsic ductility associated with increased strength of the Solution Treated and Aged condition. Ti-6A1-4V has slower crack growth rates than aluminum and somewhat faster rates than steel. In aggressive environments such as seawater, the comparative advantage of Ti-6A1-4V improves because seawater has more of an effect on the FCG rates of steel [2.4].

The fracture surface of broken FCGR coupons shows three distinct areas with their respective specific features. Zhai et al. [64] investigated the fracture surface for two types of AM Ti-6Al-4V (LENS and EBM) and for mill-annealed Ti-6Al-4V. Their fractographs are shown on Figure 2-14 and show facets in Region I and fatigue striations in Regions II and III.

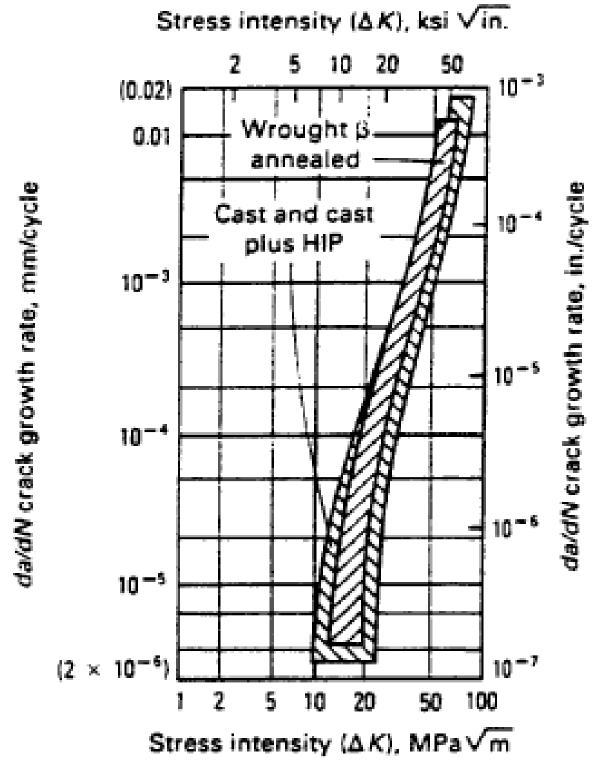


Figure 2-13: FCGR behavior of wrought and cast Ti-6Al-4V [2.4]

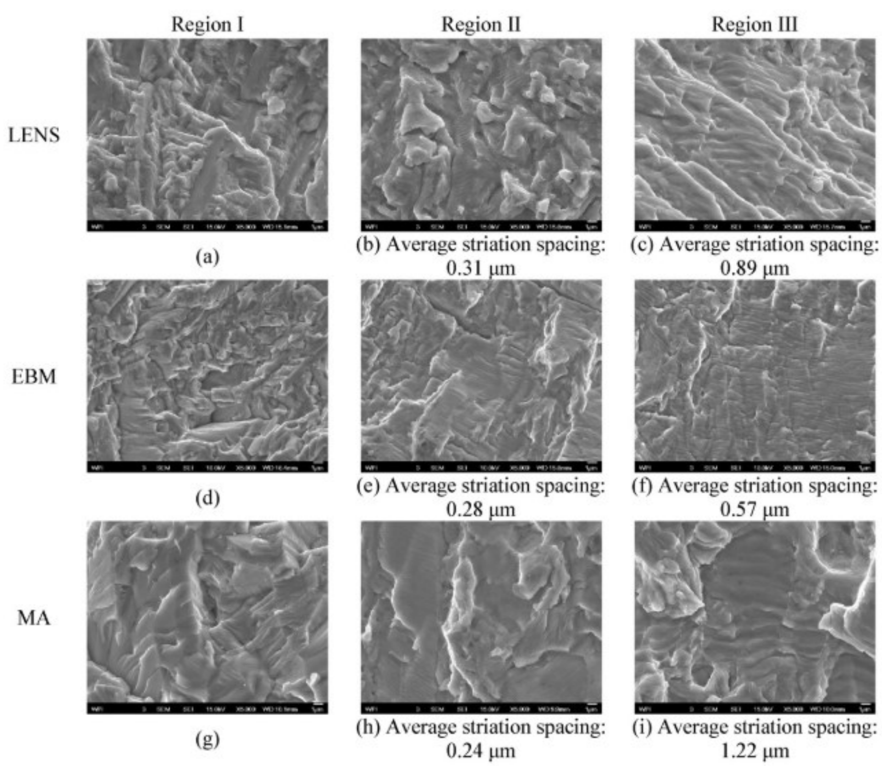


Figure 2-14: Fractographs of LENS, EBM and mill-annealed (AM) Ti-6Al-4V in Region I (a, d, g), Region II (c, f, i) and Region III of broken fatigue crack growth coupons [2.64]

### 2.3.5 Heat treatment (HT) of Ti-6Al-4V

Titanium and its alloys are heat treated for different and specific heat treatments have been developed for specific application. The main heat treatments are the following: Stress Relieving, to reduce residual stresses developed during fabrication; Annealing, to produce an optimum combination of ductility, machinability and dimension and structure stability; Solution Treating and Aging, to increase strength. Other heat treatments could be applied to optimize special properties, such as fracture toughness, fatigue strength, and high temperature creep strength [2.65].

Each Ti alloy requires different HT performed in different conditions of time, temperature and cooling depending on the process of fabrication and the component requirements. The effect of the heat treatment will depend on the alloying elements. For example, heat treatments have a limited impact on the mechanical properties of α alloys but the variety of possible microstructure in α+β alloys such as Ti-6Al-4V make them very responsive to heat treatment. [2.66] For all heat treatment above 427 °C, titanium alloys must be protected by a neutral atmosphere to prevent the formation of alpha case or contamination of oxygen or nitrogen. Donachie [2.66] suggests to take a few precautions for heat treating titanium and its alloys, defined as follow: Clean components, fixtures and furnaces prior to HT; Take care to prevent temperature from exceeding the beta transus unless specified; Remove alpha case after heat treatment; Provide sufficient stock for post-heat treatment metal removal requirements. In the case of AM Ti-6Al-4V, three kinds of HT are performed: Stress Relieving, Process Annealing or Hot Isostatic Pressure (HIP). The usual conditions of those heat treatment for Ti-6Al-4V are described in Table 2-5.

Stress-relief heat treatments decrease the undesirable residual stresses that result from the repeated thermal cycles induced during the AM process. Removal of such stresses helps maintain shape stability and eliminates unfavorable conditions such as the loss of compressive yield strength [2.66]. The different time and temperature conditions for stress relief will lead to different amount of residual stress in the final component. Figure 2-15 shows the level of residual stress in Ti-6Al-4V during stress-relief heat treatment.

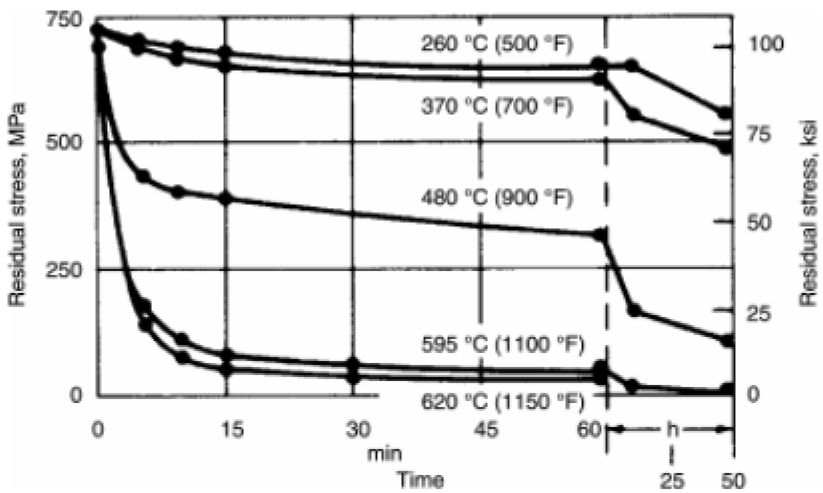


Figure 2-15: Amount of residual stress in Ti-6Al-4V depending on the time and temperature of stress-relief heat treatment [2.66]

Hot isostatic pressing (HIP) is commonly used to reduce the amount of porosity resulting from solidification shrinkage or gas porosity. This process combines annealing of the material below the β transus temperature and a uniform pressure application, in a neutral atmosphere [2.17]. Process annealing can be used to develop a balanced combination of toughness, ductility, machinability, and dimensional and structural stability. However, improving one property is usually made at the expense of another one. The most common annealing treatments performed on Ti-Al-4V are recrystallization annealing and β annealing. [2.66]

Table 2-5: Heat treatments conditions for Ti-6Al-4V, adapted from [2.65, 2.66, 2.67]

| HT | Temperature (°C) | Time (h) | Cooling method |
|---|---|---|---|
| Stress Relief | 480-650 | 1-4 | air or furnace |
| HIP (with a pressure comprised between 69 and 105 MPa) | 990-960 | 2-4 | air |
| Process Annealing | 705-790 | 1-4 | air or furnace |

## 2.4 References


[1] C. Leyens and M. Peters, *Titanium and Titanium Alloys, Fundamentals and Applications*. Wiley-VCH, 2003.

[2] G. Lütjering and J.C. Williams, *Titanium (2nd Edition)*. Springer, 2007.

[3] D. Herzog, V. Seyda, E. Wycisk and C. Emmelmann, "Additive Manufacturing of Metals," *Acta Materialia,* vol. 117, pp. 371-392, 2016.

[4] R. Boyer, G. Welsch and E.W. Collings, *Materials Properties Handbook: Titanium Alloys*. ASM International, 1994.

[5] H.W. Rosenberg, "Titanium alloying in theory and practice," presented at the The Science, Technology and Application of Titanium, 1970.

[6] R.A. Wood and R.J. Favor, *Titanium Alloys Handbook*. Metals and Ceramics Information Center, 1972.

[7] E.K. Molchanova, *Phase diagrams of Titanium alloys*. IPST, 1965.

[8] E. Brandl, A. Schoberth, C. Leyens, "Morphology, microstructure, and hardness of titanium (Ti-6Al-4V) blocks deposited by wire-feed additive layer manufacturing (ALM)," *Materials Science and Engineering A,* vol. 532, pp. 295-307, 2012.

[9] A.A. Antonysamy, "Microstructure, Texture and Mechanical Property Evolution during Additive Manufacturing of Ti-6Al-4V Alloy for Aerospace Applications," PhD, University of Manchester, 2012.

[10] *Metallurgy Additive Manufacturing for Aerospace: Market Shares, Strategies, and Forecasts, Wordwide, 2017 to 2023*. WinterGreen Reserach, 2017.

[11] *ASTM F2792-10: Standard Terminology for Additive Manufacturing Technologies*, 2010.

[12] D. Gu, *Laser additive manufacturing of high-performance materials*. Springer, 2015.

[13] I. Gibson, D. Rosen and B. Stucker, *Additive Manufacturing Technologies: 3D Printing, Rapid Prototyping, and Direct Digital Manufacturing*. Springer, New York, NY, 2015.

[14] K.M. Taminger and R.A. Hafley, "Electron beam freeform fabrication for cost effective near-net shape manufacturing," *NASA/TM-2006-214284,* 2006.

[15] B. Baufeld, E. Brandl and O. Van der Biest, "Wire based additive layer manufacturing: Comparison of microstructure and mechanical properties of Ti-6Al-4V components fabricated by laser-beam deposition and shaped metal deposition," *Journal of Materials Processing Technology,* vol. 211, pp. 1146-1158, 2011.

[16] B. Baufeld and O. Van der Biest, "Mechanical properties of Ti-6Al-4V specimens produced by shaped metal deposition," *Science and Technology of Advanced Materials,* vol. 10, 2009.

[17] F.H. Froes and B. Dutta, "The Additive Manufacturing (AM) of Titanium alloys," vol. 1019, pp. 673-679, 2014.

[18] B. Baufeld, O. Van der Biest and R. Gault, "Additive manufacturing of Ti-6Al-4V components by shaped metal deposition: Microstructure and mechanical properties," *Materials and Design,* vol. 31, pp. 5106-5111, 2010.

[19] E. Brandl, C. Leyens and F. Palm, "Mechanical Properties of Additive Manufactured Ti-6Al-4V Using Wire and Powder Based Processes," presented at the IOP Conf. Series: Materials Science and Engineering, 2011.
[20] E. Brandl, V. Michailov, B. Viehweger and C. Leyens, "Deposition of Ti-6Al-4V using laser and wire, part I: Microstructural properties of single beads," *Surface & Coatings Technology,* vol. 206, pp. 1120-1129, 2011.
[21] E. Brandl, F. Palm, V. Michailov, V. Viehweger, C. Leyens, "Mechanical properties of additive manufactured titanium (Ti-6Al-4V) blocks deposited by a solid-state laser and wire," *Materials and Design,* vol. 32, pp. 4665-4675, 2011.
[22] E. Brandl, B. Baufeld, C. Leyens and R. Gault, "Additive manufactured Ti-6Al-4V using welding wire: comparison of laser and arc beam depostion and evaluation with respect to aerospace material specifications," *Physics Procedia,* vol. 5, pp. 595-606, 2010.
[23] E. Brandl, V. Michailov, B. Viehweger and C. Leyens, "Deposition of Ti-6Al-4V using laser and wire, part II: Hardness and dimensions of single beads," *Surface & Coatings Technology,* vol. 206, pp. 1130-1141, 2011.
[24] B.E. Caroll, T.A. Palmer and A.M. Beese, "Anisotropic tensile behavior of Ti-6Al-4V components fabricated with direct energy deposition additive manufacturing," *Acta Materialia,* vol. 87, pp. 309-320, 2015.
[25] P.A. Kobryn, E.H. Moore and S.L. Semiatin, "The effect of Laser Power and Transverse speed on Microstructure, Porosity, and Build Height in Laser-Deposited Ti-6Al-4V," *Scripta mater.,* vol. 43, pp. 299-305, 2000.
[26] N. Shamsaei, A. Yadollahi, L. Bian and S.M. Thompson, "An overview of Direct Laser Deposition for additive manufacturing; Part II: Mechanical behavior, process parameter optimization and control," *Additive Manufacturing,* vol. 8, pp. 12-35, 2015.
[27] J. Mazumder, D. Dutta, N. Kikuchi and A. Ghosh, "Closed loop direct metal deposition: art to part," *Optics and Lasers in Engineering,* vol. 34, pp. 397-414, 2000.
[28] M.L. Griffith et al., "Understanding thermal behavior in the LENS process," *Materials and Design,* vol. 20, pp. 107-113, 1999.
[29] P.A. Kobryn and S.L. Semiatin, "Microstructure and texture evolution during solidification processing of Ti-6Al-4V," *Journal of Materials Processing Technology,* vol. 135, pp. 330-339, 2003.
[30] B. Zheng, Y. Zhou, J.E. Smugeresky, J.M. Schoenung and E.J. Lavernia, "Thermal behavior and microstructure evolution during laser deposition with laser-engineered net shaping: Part II. Experimental investigation and discussion," *Metallurgical and Materials Transactions A,* vol. 39, pp. 2237-2245, 2008.
[31] G.P. Dinda, A.K. Dasgupta and J. Mazumder, "Laser aided direct metal deposition of Inconel 625 superalloy: microstructural evolution and thermal stability," *Materials Science & Engineering A,* vol. 509, pp. 98-104, 2009.
[32] L. Costa, R. Vilar, T. Reti and A.M. Deus, "Rapid tooling by laser powder deposition: process simulation using finite element analysis," *Acta Materialia,* vol. 53, pp. 3987-3999, 2005.
[33] *ASTM E6-09be1 Standard terminology relating to methods of mechanical testing*, 2009.
[34] A.J. Pinkerton, W. Wang and L. Li, "Component repair using laser direct metal deposition," *Proc. IMechE, Part B: J. Engineering Manufacture,* vol. 222, 2007.

[35] T. Marazani, D.M. Madyira, E.T. Akinlabi, "Repair of cracks in metals: A review," *Procedia Manufacturing,* vol. 8, pp. 673-679, 2017.
[36] B. Graf, A. Gumenyuk, M. Rethmeier, "Laser metal deposition as repair technology for stainless steel and titanium alloys " *Physics Procedia,* vol. 39, pp. 376-381, 2012.
[37] S. Kou, *Welding Metallurgy, Second Edition*. John Wiley & Sons Inc, 2003.
[38] Nanda Kumar Dey, "Additive Manufacturing laser deposition of Ti-Al-4V for aerospace repair application," Masters, Missouri University of science and Technology, 2014.
[39] R. Delhoff, C. Duty, W. Peter, Y. Yamamoto and W. Chen, "Case Study: Additive Manufacturing of Aerospace Brackets," *Advanced Materials and Processes,* vol. 171, pp. 19-22, 2013.
[40] G.A. Sargent, K.T. Kinsel, A.L. Pilchak, A.A. Salem and S.L. Semiatin, "Variant Selection During Cooling after Beta Annealing of Ti-6Al-4V Ingot Material," *Metallurgical and Materials Transactions A,* vol. 43, pp. 3570-3585, 2012.
[41] *AMS4999A: Titanium Alloy Direct Deposited Product 6Al-4V Annealed*, 2011.
[42] *ASTM F1472-14: Standard Specification for Wrought Titanium-6Aluminum-4Vanadium Alloy for Surgical Implant Applications*, 2014.
[43] S.A. David and J.M. Vitek, "Correlation between solidification parameters and weld microstructure," *International Materials Reviews,* vol. 34, no. 5, pp. 213-245, 1989.
[44] D.A. Porter, K.E. Easterling, M.Y. Sherif, *Phase Transformations in Metals and Alloys, Third Edition*. CRC Press, 2009.
[45] S.L. Semiatin, S.L. Knisley, P.N. Fagin, F. Zhang and D.R. Barker "Microstructure and texture evolution during solidification processing of Ti–6Al–4V," *Journal of Materials Processing Technology,,* vol. 135, pp. 330-339, 2003.
[46] S.M. Kelly and S.L. Kampe, "Microstructural Evolution in Laser-Deposited Multilayer Ti-6Al-4V Builds: Part I. Microstructural Characterization," *Metallurgical and Materials Transactions A,* vol. 35, pp. 1861-1867, 2004.
[47] M. Borlaug Mathisen, L. Eriksen, Y. Yu, O. Jensrud and J. Hjelen, "Characterization of microstructure and strain response in Ti–6Al–4V plasma welding deposited material by combined EBSD and in-situ tensile test," *Transactions of Nonferrous Metals Society of China,* vol. 24, pp. 3929-3943, 2014.
[48] A.R. Nassar and E.W. Reutzel, "Additive Manufacturing of Ti-6Al-4V Using a Pulsed Laser " *Metallurgical and Materials Transactions A,* vol. 46, pp. 2781-2789, 2015.
[49] C. Qiu et al., "Fabrication of large Ti-6Al-4V structures by direct laser deposition," *Alloys and Compounds,* vol. 619, pp. 351-361, 2015.
[50] G.E. Totten, M.A.H. Howes and T. Inoue, *Handbook of Residual Stress and Deformation of Steel*. ASM International, 2002.
[51] C.R. Knowles, "Residual Stress Measurement and Structural Integrity Evaluation of SLM Ti-6Al-4V," MSc, University of Cape Town, 2012.
[52] J-P Kruth, M.C. Leu and T. Nakagawa, "Progress in Additive Manufacturing and Rapid Prototyping," *CIRP Annals - Manufacturing Technology,* vol. 47, pp. 525-540, 1998.
[53] J.J. Lewandowski and M. Seifi, "Metal Additive Manufacturing: A review of Mechanical properties," *Annual Review of Materials Research,* vol. 46, no. 151-186, 2016.
[54] *ASTM F1108: Standard Specification for Titanium-6Aluminum-4Vanadium Alloy Castings forSurgical Implants (UNS R56406)*, 2014.

[55] *ASTM F2924:Standard Specification for Additive Manufacturing Titanium-6Aluminum-4Vanadium with Powder Bed Fusion*, 2012.
[56] P.A. Kobryn and S.L. Semiatin, "Mechanical Properties of Laser-Deposited Ti-6Al-4V," *AFRL/MLLMP,* pp. 179-186, 2002.
[57] S.H. Mok et al., "Deposition of Ti-6Al-4V using a high power diode laser and wire, part II: Investigation on the mechanical properties," *Surface & Coatings Technology,* vol. 202, pp. 4613-4619, 2008.
[58] E. Amsterdam and G.A. Kool, "High cycle fatigue of laser beam deposited Ti-6Al-4V and Inconel 718," presented at the 25th ICAF Symposium: Bridging the Gap between Theory and Operational Practice, 2009.
[59] B. Baufeld, "Effect of deposition parameters on mechanical properties of shaped metal deposition parts," *Proc. IMechE, Part B: J. Engineering Manufacture,* vol. 226, pp. 126-136, 2012.
[60] F.C. Campbell, *Fatigue and fracture: understanding the basics*. ASM International, 2012.
[61] V.A. Joshi, *Titanium alloys: an atlas of structures and fracture features*. CRC Press, 2006.
[62] *ASTM E647: Standard Test Method for Measurements of Fatigue Crack Growth Rates*, 2015.
[63] R.I. Stephens and H.O. Fuchs, "Metal Fatigue in Engineering," New York: Wiley, 2001.
[64] Y. Zhai, H. Galarraga and D.A. Lados, "Microstructure, static properties, and fatigue crack growth mechanisms in Ti-6Al-4V fabricated by additive manufacturing: LENS and EBM," *Engineering Failure Analysis,* vol. 69, pp. 3-14, 2016.
[65] ASM International, *Metals Handbook*. 1998.
[66] M. J. Donachie, *Titanium: a technical guide*. Materials Park, OH : ASM International, 2000.
[67] *ASM2801B: Heat Treatment of Titanium Alloy Parts*, 2014.

# Chapitre 3 - Material and experimental procedure

This section will discuss the general techniques used for the research presented in this work later discussed in Chapter 4. The material, fabrication technique, and the characterisation used will be presented in this chapter.

## 3.1 Sample fabrication

The samples produced for this work were built using a LAWS 1000 automated deposition system at Liburdi (Hamilton, ON, Canada) presented on Figure 3-1. An IPG fiber laser (IPG Photonics, Oxford) reaching up to 1kW power is used to fuse the material. To prevent excessive oxidation, all deposits are completed in an argon inert environment.


Figure 3-1: Liburdi LAWS 1000 automated deposition system [3.1]

The printing strategy is shown on Figure 3-2. The deposition of a bead starts and ends always on the same opposite sides. Each deposited layer for the thick specimens were made of nine lateral beads with a predefined hatch spacing equivalent to 50% of a single bead width.

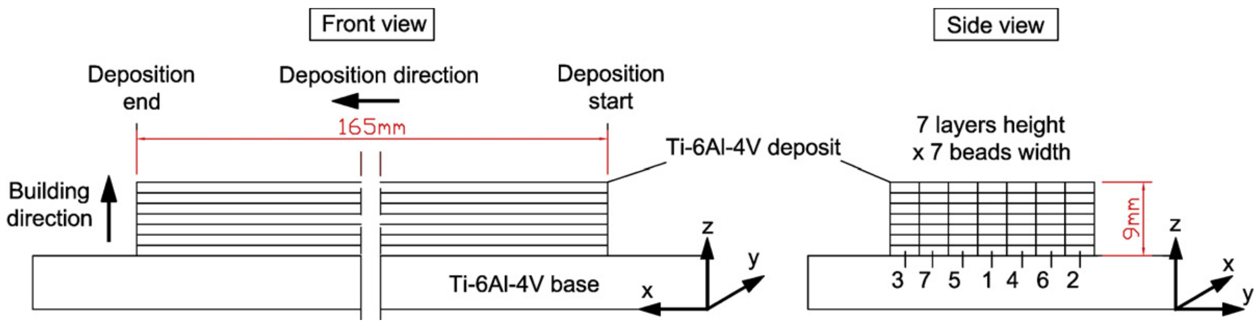


Figure 3-2: Schematic strategy of printing [3.2]

The feeding material used is a Ti-6Al-4V wire spool with Extra-Low Interstitials which was deposited on wrought Ti-6Al-4V substrates. Alloying elements and typically measured impurities of the wire spool and the substrate are shown in Table 3-1.

Table 3-1: Typical composition of the selected Ti-6Al-4V wire spool and substrate

| | Alloying Elements wt% max | | Impurities wt% max | | | | |
|---|---|---|---|---|---|---|---|
| | Al | V | N | C | H | Fe | O |
| Wire | 6.28 | 4.24 | 0.0027 | 0.01 | 0.001 | 0.025 | 0.045 |
| Substrate | 6.53 | 4.00 | 0.009 | 0.017 | 0.0056 | 0.176 | 0.1740 |

All specimens went through a stress relief heat treatment during 2h at 593°C followed by air cooling, accordingly to the AMS2801 specification [3.3], to remove the residual stress induced by the thermal history of the process.

## 3.2 Sample preparation

The samples received from Liburdi (ON, Canada) were sectioned and prepared for metallographic observation. The sectioning was accomplished in two steps: first, large cuts performed with an abrasive saw and then precision cuts made with a diamond blade saw. The samples were then mounted in conductive resin to be ground and polished.

Grinding was performed on sandpaper with water and the steps were the following: 240 grit SiC, 320 grit SiC, 400 grit SiC, 600 grit SiC, 800 grit SiC, followed by 1200 grit SiC. Polishing was made using 0.05 µm colloidal silica on a Vibromet apparatus (Buehler Vibromet2, Düsseldorf, Germany).

In order to bring out the general alpha-beta microstructure for optical microscopy, the samples were etched using a Kroll's reagent, made of 2% hydrofluoric acid (HF), 6% nitric acid ($HNO_3$) and 92% water [3.4]. The samples were submerged in the etchant for 15 s.

## 3.3 Microscopy

A Nikon light optical microscope coupled with Clemex Vision System was used for microstructural examination on etched samples up to a magnification of x1000. Preliminary observations were made on unetched samples, to evaluate the presence of defects.

High magnification microstructural examination and fracture surface observations were performed through scanning electron microscopy with a Hitachi SU3500 SEM (Hitachi, Tokyo, Japan) shown in Figure 3-3. Investigations of the microstructure were performed using Back-Scattered Electrons at 20kV and fractographs were obtained at 20kV with Secondary Electrons.

Figure 3-3: Hitachi SU3500 SEM [3.5]

## 3.4 Mechanical characterization

Vickers microhardness was measured on polished and unetched samples using a Clark Microhardness (CM-100AT) Indenter, with 500 gf and a 15 s indentation period. The hardness measurements reported were averages of 10 measurements, in order to ensure representative values. The hardness profile of the interface was obtained from indentations performed every 125µm on lines perpendicular from the interface line.

The samples produced for mechanical testing were sent to EXOVA who machined and tested them. Two kinds of tests were performed: static tensile testing and fatigue crack growth rate (FCGR).

Static tensile tests were realized accordingly to the ASTM E8 standard [3.6] at room temperature at 0.005 mm/mm/min past yield and then 0.05 mm to fracture. The tensile coupons shown on Figure 3-4 have a gage diameter of 6 mm and a gage length of 30 mm. The material was tested in two directions: longitudinal direction (X) which is the deposition direction and transverse direction (Z) which is the building direction.

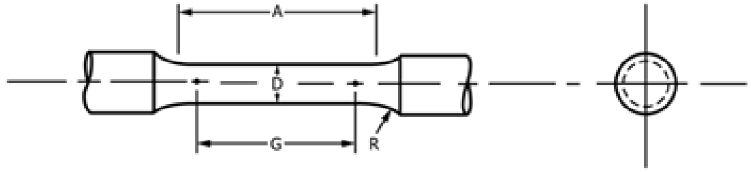


| | Specimen Dimensions (mm) |
|---|---|
| G – Gage length | 30 |
| D – Diameter | 6 |
| R – Radius of fillet, min | 6 |
| A – length of reduced section, min | 36 |
| Diameter of end section | 12 |
| Overall length | 60 |

Figure 3-4: Tensile coupons geometry [3.6]

FCGR tests were performed accordingly to the ASTM E647 standard [3.7] using Direct Current Potential Drop techniques for crack length measurement. Test specimens geometry is described on Figure 3-5. Tests were performed at R=0 at room temperature using 50 Hz and C=-6 down to threshold and 20 Hz during the K increasing portion of the curve. Precracking was at a delta K level of 8 to 11 MPa√m to a crack length of 13 mm (nominal) prior to starting the threshold portion of the test. After threshold was determined, the Paris region of the curve was determined starting from approximately 8 MPa√m.

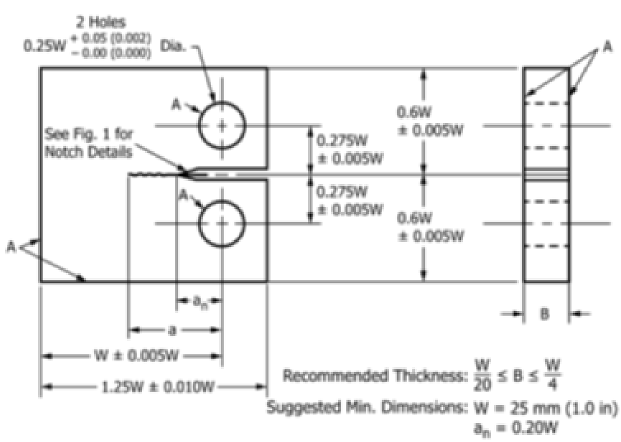


| | Specimen Size (mm) |
|---|---|
| Thickness | 13 |
| Length | 60 |
| Width | 64 |
| Crack length | 23 |

Figure 3-5: FCGR coupons geometry [3.7]

## 3.5 References


[1] Liburdi Engineering. Available: http://liburdi.com/welding-systems-automation-automated-welding-systems-laws-1000

[2] E. Brandl, A. Schoberth, C. Leyens, "Morphology, microstructure, and hardness of titanium (Ti-6Al-4V) blocks deposited by wire-feed additive layer manufacturing (ALM)," *Materials Science and Engineering A,* vol. 532, pp. 295-307, 2012.

[3] *ASM2801B: Heat Treatment of Titanium Alloy Parts*, 2014.

[4] Luther M. Gammon et al., "Metallography and Microstructure of Titanium and its Alloys," in *ASM Handbook, Volume 9: Metallography and Microstructures*, 2004, pp. 899-917.

[5] Hitachi High-Technologies Corporation. Available: https://www.hitachi-hightech.com/global/product_detail/?pn=em-su3500

[6] *ASTM E8/E8M: Standard Test Method for Tension Testing of Metallic Materials*, 2016.

[7] *ASTM E647: Standard Test Method for Measurements of Fatigue Crack Growth Rates*, 2015.

# Chapitre 4 - Microstructure and Fatigue crack growth of Direct Energy Deposited Ti-6Al-4V

## Preface

Microstructure and Fatigue crack growth of Direct Energy Deposited Ti-6Al-4V is a comprehensive work which includes all experimental procedures and expected results outlined in Chapter 4. This paper is intended to be published in a scientific journal during the 2018 year. Results for microstructure analysis and mechanical properties are presented in detail and will be discussed in this chapter. The citation of this article is as follows:

F. Chainiau, Y. Ding and M. Brochu. Microstructure and Fatigue crack growth of Direct Energy Deposited Ti-6Al-4V. Article intended for publication. 2018.

## 4.1 Abstract

Additive Manufacturing (AM) is of growing interest to produce and repair components, especially for the aerospace industry, which uses costly materials such as titanium alloys. In this paper, the microstructure and mechanical properties of AM produced Ti-6Al-4V in a repair context are investigated and discussed. Simulated repair coupons were produced on Ti-6Al-4V wrought substrate using Ti-6Al-4V ELI grade wire with the direct energy deposition process. Characterization campaigns led to the evaluation of the microstructure, hardness, tensile behavior and fatigue crack growth resistance of the build-up metal, along with a microstructural and hardness analysis of a simulated repaired interface. The experiments reveal that the deposited material meets all standard requirements, but the repair region shows evolving mechanical behavior.

## 4.2 Introduction

The aerospace industry is facing several challenges to cover the increasing air traffic. Numerous researches have been and are still conducted to face those challenges, focusing on both materials and processes [4.1]. This led to the development of specific aerospace alloys such as titanium alloys, which offers exceptional balance of strength, ductility, fatigue and fracture properties [4.2]. Titanium can be found in airfcraft applications such as airframe or gas turbine engines, but also in helicopters and spacecraft [4.3]. Among the variety of titanium alloys, Ti-6Al-4V is the most commonly used [4.4]. However, in addition to the high cost of the raw material, Ti-6Al-4V can lead to important financial expenditures during the maintenance and traditional repair procedures for such parts.

Several techniques for repairing metal components have been studied [4.5] to increase the life cycle of components. Among them is Direct Energy Deposition (DED), an additive manufacturing (AM) process that is also referred as Laser Metal Deposition [4.6, 4.7, 4.8]. DED uses laser to melt a small amount of metal fed into the laser beam and deposited on a substrate, in a layer by layer methodology [4.9]. This process can use either wire- or powder-feedstock. Wire was introduced to overcome some issues linked to the use of powder such as contamination (oxygen) and cost of high-quality powders [4.10]. DED processes have been studied as a repair technique for several years for steels [4.6] and more recently for titanium alloys (with powder-feedstock) [4.7, 4.8].

Titanium alloys are very sensitive to the thermal history induced by the manufacturing process so the microstructure and final mechanical properties are highly influenced by the manufacturing sequence [4.11, 4.12]. Different microstructures can be obtained in this $\alpha+\beta$ alloy [4.13]. The cooling transformation $\beta \rightarrow \alpha + \beta$, which occurs at 1000 °C for Ti-6Al-4V [4.2], can lead to a large variety of microstructures influenced by the fabrication process and the cooling rate. Particularly, when this alloy is additively manufactured, each layer sees repeated heating cycles with high cooling rates leading to the formation of different microstructures [4.14]. In AM parts, the solidification growth direction is perpendicular to the solid/liquid interface, resulting in the growth of columnar grains aligned with the thermal gradient [4.15]. These microstructural features induce anisotropy in the tensile behavior of the material and different crack propagation behavior as the crack growth and threshold are dependent on the direction of crack propagation [4.16]. Typical DED wire reports have shown that a Widmanstätten microstructure develops during fabrication [4.17]. In the context of a repair, imposing such thermal profile and material addition on wrought or cast Ti-6Al-4V substrate can create additional mismatch in microstructure. A commonly used solution is performing heat treatment to homogenize the repaired part after the AM deposition, but this avenue can yield significant distortions in the part [4.18]. A few studies focused on the feasibility of the repair [4.5, 4.6, 4.7, 4.8, 4.19] which defined building strategies that were able to properly fill grooved shapes [4.6, 4.7] and initiated the characterisation of the repaired structure through microstructural analysis [4.7] and tensile testing of the repaired interface [4.8]. However, the published works related to the use of DED as a repair techniques are too few to state the mechanical behavior of the overall repaired component [4.5].

The objective of this work is to study the microstructure and mechanical properties of AM Ti-6Al-4V in the context of a repaired component. Mechanical tests include hardness, tensile testing and fatigue crack growth rate. The only heat treatment considered in this work was stress relief, in order to remove the residual stress induced in the repaired part by the thermal cycle impose by the AM process while having minimal effect on part distortion.

## 4.3 Experimental procedure

The samples for this work were produced using a LAWS 1000 automated deposition system at Liburdi (Hamilton, ON, Canada). An IPG Yb:YAG fiber laser (IPG Photonics, Oxford) reaching up to 1kW power is used to fuse the material. The feeding material used is a Ti-6Al-4V wire spool with Extra-Low Interstitials, which was deposited on rolled annealed grade 5 Ti-6Al-4V substrates. To prevent excessive oxidation, all deposits are completed in an argon inert environment. All specimens undergo a stress relief heat treatment during 2h at 593°C followed by air cooling, accordingly to AMS2801 [4.20].

For microstructural evaluation, the received specimens were sectioned, mounted, ground up to 1200 grit SiC paper, and finally polished with colloidal silica. For optical observations, the samples were etched with a Kroll's reagent made of 2% HF, 6% $HNO_3$ and 92% $H_2O$. [4.20]

A Nikon light optical microscope coupled with Clemex Vision System was used for microstructural examination on etched samples. Preliminary observations were made on unetched samples, to evaluate the presence of defects. High magnification microstructural examination and fracture surface observations were performed through scanning electron microscopy using a Hitachi SU3500 SEM (Hitachi, Tokyo, Japan). Alpha plate thickness and the size of the prior β grains were measured with ImageJ software accordingly to the ASTM E112 standard [4.21].

Vickers microhardness was measured using a Clark Microhardness (CM-100AT) Indenter, with 500 gf and a 15 s indentation period, on polished and unetched samples. The hardness measurements reported were averages of 10 measurements, in order to ensure representative values. The hardness profile of the interface was obtained from indentations performed every 125µm on lines perpendicular from the interface line.

The samples produced for mechanical testing were sent to EXOVA. Two campaigns of tests were performed: static tensile testing and fatigue crack growth (FCGR). Tensile tests were realized accordingly to the ASTM E8 standard [4.22]. The material was tested in two directions relative to build direction: longitudinal direction (X) and transverse direction (Z). FCGR tests were performed accordingly to the ASTM E647 standard [4.23] using Direct Current Potential Drop techniques for crack length measurement. Tests were performed at R=0 at room temperature using 50 Hz and C=-6 down to threshold and 20 Hz during the K increasing portion of the curve. Precracking was at a delta K level of 8 to 11 MPa√m to a crack length of 13 mm (nominal) prior to starting the threshold portion of the test. After threshold was determined, the Paris region of the curve was determined starting from approximately 8 MPa√m.

## 4.4 Results & Discussion

### 4.4.1 Morphology and microstructure

Figure 4-1 shows one of the blocks produced by DED. The surface of the blocks shows largely shiny areas combined with dull, brown, and blue areas, similarly to what observed Brandl [4.4]. This colorization indicates a thin oxide layer despite the high purity of the argon atmosphere. It is yet believed that this coloration is only a surface defect and does not affect the properties of the component [4.14]. Figure 4-1 shows a general micrograph of the etched cross section of the block.

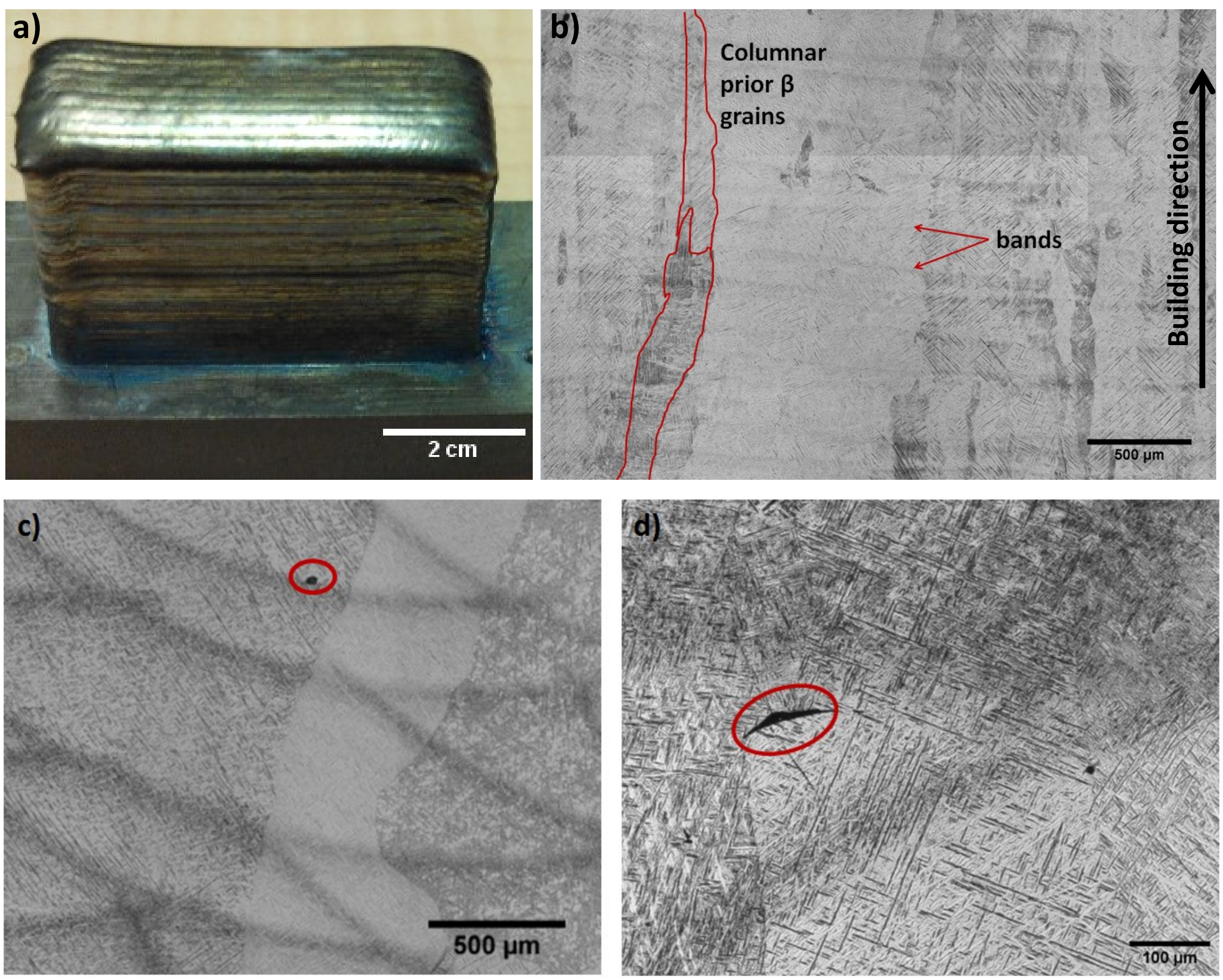


Figure 4-1: a) Ti-6Al-4V stress relieved block produced by DED; b) Mosaic of the etched cross section of the block; Defects in DED printed Ti-6Al-4V: c) pore, d) lack of fusion

During the deposition, epitaxial grain growth mainly occurs through heterogeneous nucleation as both substrate and filler metals are of the same composition [4.24]. During the solidification process, grains tend to grow perpendicular to the solid/liquid interface, which results in the formation of columnar grains. [4.13, 4.15] The axes of the columnar grains are approximately parallel to the *Z*-axis, *i.e.*, the build direction of the deposit. [4.25] From the built up material, an average width of 405 ±120 µm was measured for the prior β grains for a length of a few millimeters. The reported prior β grains size varies throughout the literature and is function of the process conditions used and printed geometry [4.11, 4.24, 4.26] as the formation of the grains depends on the thermal cycle induced by the process. Caroll et al. [4.26] obtained similar prior β grains size with their powder DED process. Baufeld [4.11] reported that for wire DED using lower speed and laser current, that wider prior β grains are obtained.

The observed parallel bands have a height of 666.6 ±5 µm. The formation of bands is widely observed throughout the literature [4.14, 4.24, 4.26, 4.27, 4.28, 4.29, 4.30, 4.31, 4.32], where the spacing of the bands varies from 766 µm to 3mm, depending on the process parameters. Those bands are attributed to the alpha/beta transformation at the β transus temperature [4.14]. The microstructure between the bands as depicted in Figure 4-2, consists of basketweave Widmmanstätten α phase in retained β phase and the microstructure within the bands is characterized by larger colonies of acicular α [4.24]. The top of the uppermost parallel band indicates the β transus line during the last DED step and the bands below result from β transus lines from previous DED steps. Kelly and Kampe have modeled this in detail [4.24, 4.33]. They established that up to the three previous layers affect the thermal behavior of a newly deposited layer. However, their model only was limited to characterizing the thermal history form the previous layer. Based on Kelly's work among others, Irwin et al. [4.34] created a model which was validated for properties and microstructural features prediction and which also simulated the band formation. This would validate the fact each layer's thermal cycle is influenced by the three previous layers and influences the next three layers, leading to a band free area at the top of the build that would be three layers high. This agrees with the current work.

Defects such as porosity developed during DED process are some of the most common issues associated with DED of Ti–6Al–4V [4.35], even though the porosity level in DED produced parts is very low. Two types of porosity can be find within DED produced samples: interlayer and intralayer porosity [4.32, 4.36]. Those two types of defects are illustrated on Figure 4-1. The specimens studied in this work show a level of porosity of 0.12 ± 0.045 % per area. Kobryn et al. [4.32] suggested that intralayer porosities were gas pores, generally spherical, generated by gas entrapment during the deposition and interlayer porosity usually form at the interface of layers due to lack of fusion and show elongated or irregular-shaped morphology.. The usual level of gas porosity in DED parts in lower than 0.05% whiles the amount of lack-of-fusion porosity greatly varies. An overall level of porosity below 0.20 % per area has negligible effect on the deposits behavior [4.37].

DED has a major impact on the morphology and the microstructure of Ti-6Al-4V that is recurrently characterized by two macrostructures shown on Figure 4-1: columnar prior β grains and layer bands.

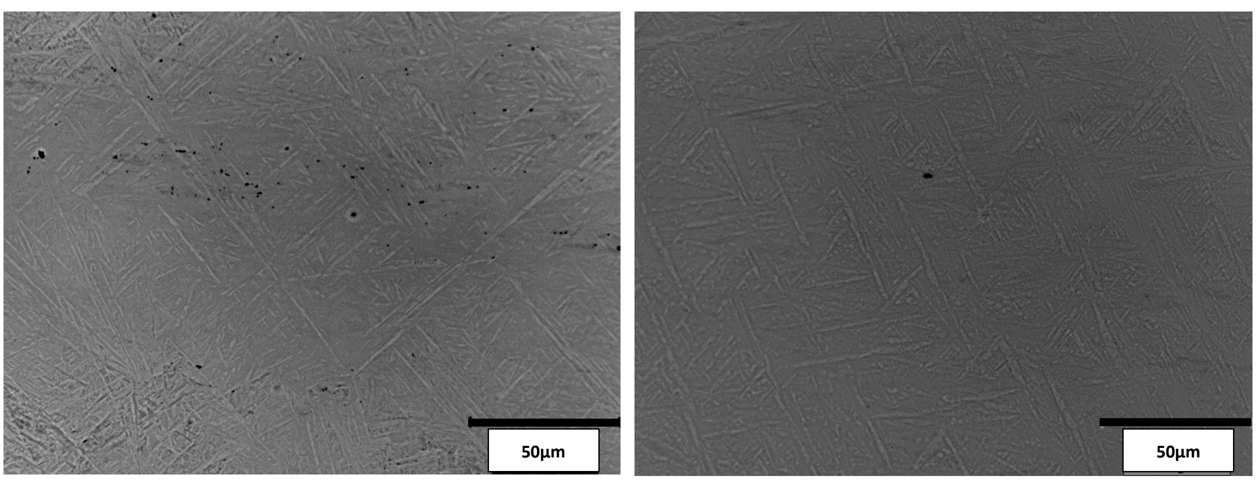


Figure 4-2: a) microstructure between the bands; b) microstructure of the bands

The microstructure show in Figure 4-3, consists of α platelets in a β matrix [4.30]. A Widmanstätten structure developed in the AM part that is slightly coarser at the bottom of the part (close to the build plate) resulting from the thermal cycle imposed by the DED process. An average alpha plate thickness of 1.16 ±0.25 µm was measured at the bottom, compared to 0.8 ±0.1 µm from the top.

The larger Widmanstätten structure size at the bottom of the deposit has been reported in previous studies [4.14, 4.24, 4.35, 4.36]. In the first deposited layers, the added material underwent repeated thermal gyration in the α+β phase field, allowing the diffusive element partition resulting into the coarsening of the α lamellae [4.14]. During the deposition of the final layer, the melted material solidifies in the β field and transforms into a fine Widmanstätten structure at a fast cooling rate. Kelly [4.24] modelled the evolution of the microstructure of the different layer showed on Figure 4-4 and established that the cooling rate of the final layer was around 32 K/s. They measured an average alpha thickness of 0.90 ±0.38 µm at the top of the build and 1.57 ±0.59µm at the bottom of the build. Since the alpha size is similar to the one measured in this work, we can expect a similar cooling rate.

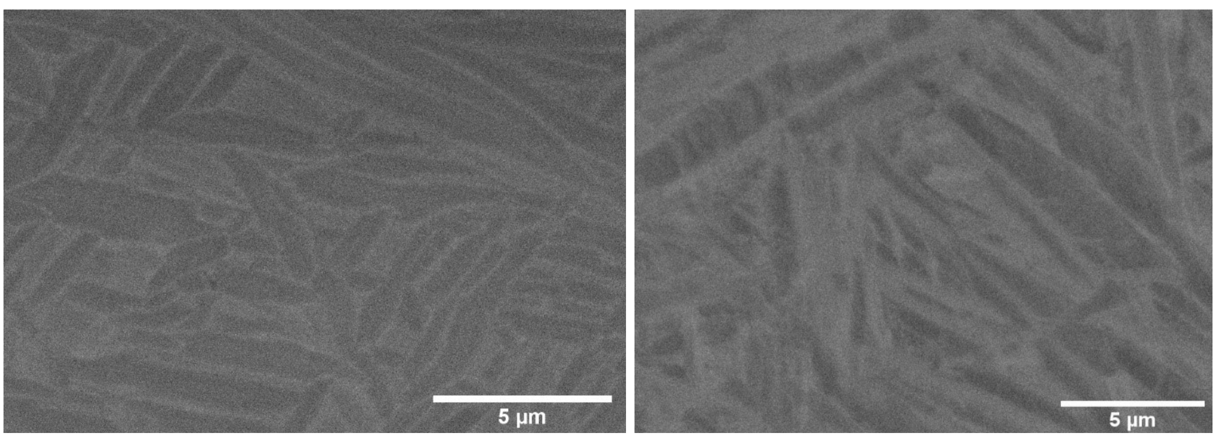

Figure 4-3: Alpha thickness and SEM micrographs of the microstructure in different regions of the samples; a) Top of the part (last deposited layers), b) Bottom of the part (first deposited layers, close to the build plate)

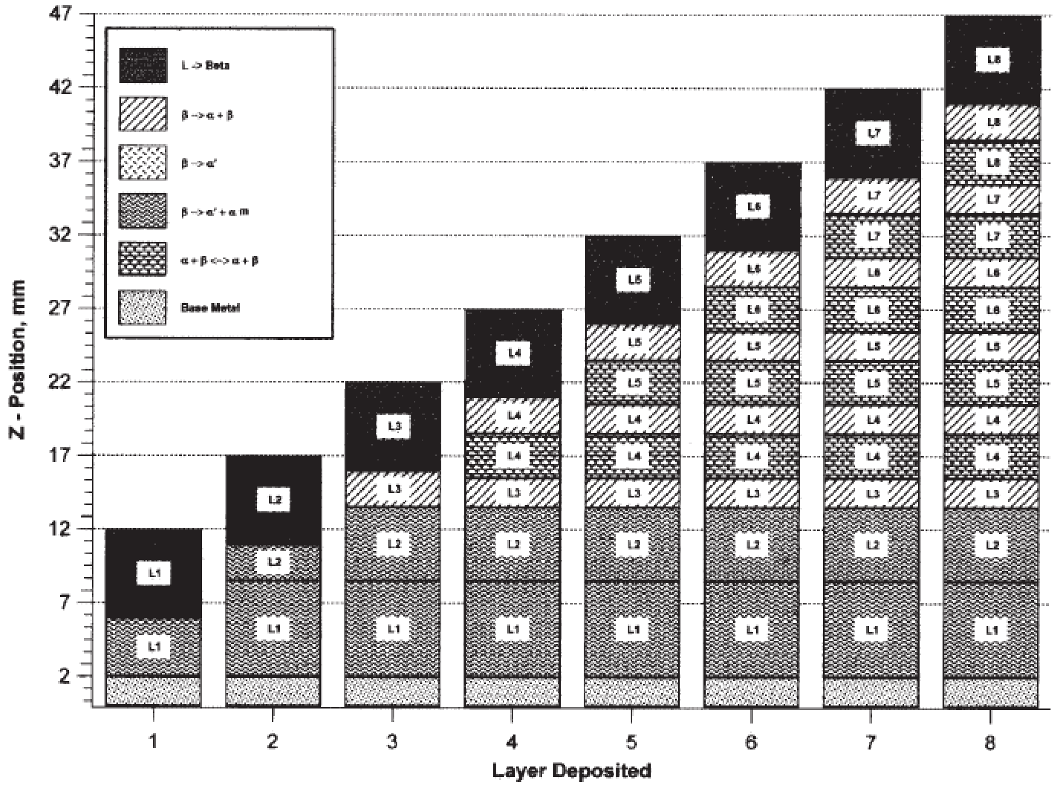


Fig. 11—Microstructural evolution map of the build as each layer is deposited. Each morphology is indicated by a different fill pattern and labeled as to what layer deposition "L*n*" is responsible for its formation. The position of each layer is indicated by horizontal gridlines.

Figure 4-4: Microstructural evolution map of laser deposited Ti-6Al-4V [4.33]

### 4.4.2 Hardness

Hardness tests were first performed on a block identical to those from which the coupons were extracted. The block was stress relieved for 2h at 593°C followed by air cooling. Measurements were done on the cross-section perpendicular to the deposition direct for the bottom (near the substrate) to the top of the specimen (last deposited layers). Tests were then performed on the grips of a tensile coupon. A coupon tested in the X direction was selected in order to measure its hardness in the first deposited layers (bottom) and last deposited layers (top). Hardness measurements are reported on Table 4-1. The hardness of the substrate before stress relief as reported by the substrate manufacturer was 320 HV.

Table 4-1: Hardness of DED Ti-6Al-4V

| | Top | Bottom |
|---|---|---|
| Block | 320.6 ±7 HV | 323.4 ±17 HV |
| Tensile coupon | 321.2 ±4 HV | 326.7 ±4 HV |

Despite the difference in the alpha thickness throughout the height of the built, no statistical difference in hardness was observed between the top and the bottom of the built in both the block and the tensile coupon, similarly to what found Baufeld and Brandl [4.4, 4.14]. Since the hardness is related to strength, not much variation in the tensile properties throughout the DED part height is to be expected. The hardness of wrought or cast annealed Ti-6Al-4V is in the surrounding of 350 HV [4.38] and DED parts hardness has been reported to vary between 296 and 365 HV [4.4, 4.11, 4.14, 4.26, 4.39]. In DED produced and stress relieved parts, the hardness tend to be lower than the hardness of the wrought or cast annealed alloy as the columnar grains formed by the thermal cycles are bigger than the grains of the bimodal structure observed in annealed wrought or cast Ti-6Al-4V. The hardness is also impacted by the size of the α platelets. Tan et al. [4.40] reported that larger α platelets would lead to a reduces hardness. The highest value obtained in the literature for DED processes using powder or wire are generally obtained after a faster cooling rate leading to the formation of a martensitic structure.

### 4.4.3 Tensile properties

Figure 4-5 and Figure 4-6 summarize the tensile tests results compared to existing values from the literature and provide the required properties specified in the AMS4999A standard [4.41] related to the DED Ti-6Al-4V products. All the coupons tested match the requirements for DED Ti-6Al-4V (represented by the horizontal and vertical lines). Picture depicting fractured coupons is shown on Figure 4-7. The tensile behavior was tested in two directions in order to assess the anisotropy of the material induced by the directed microstructure of AM produced parts.

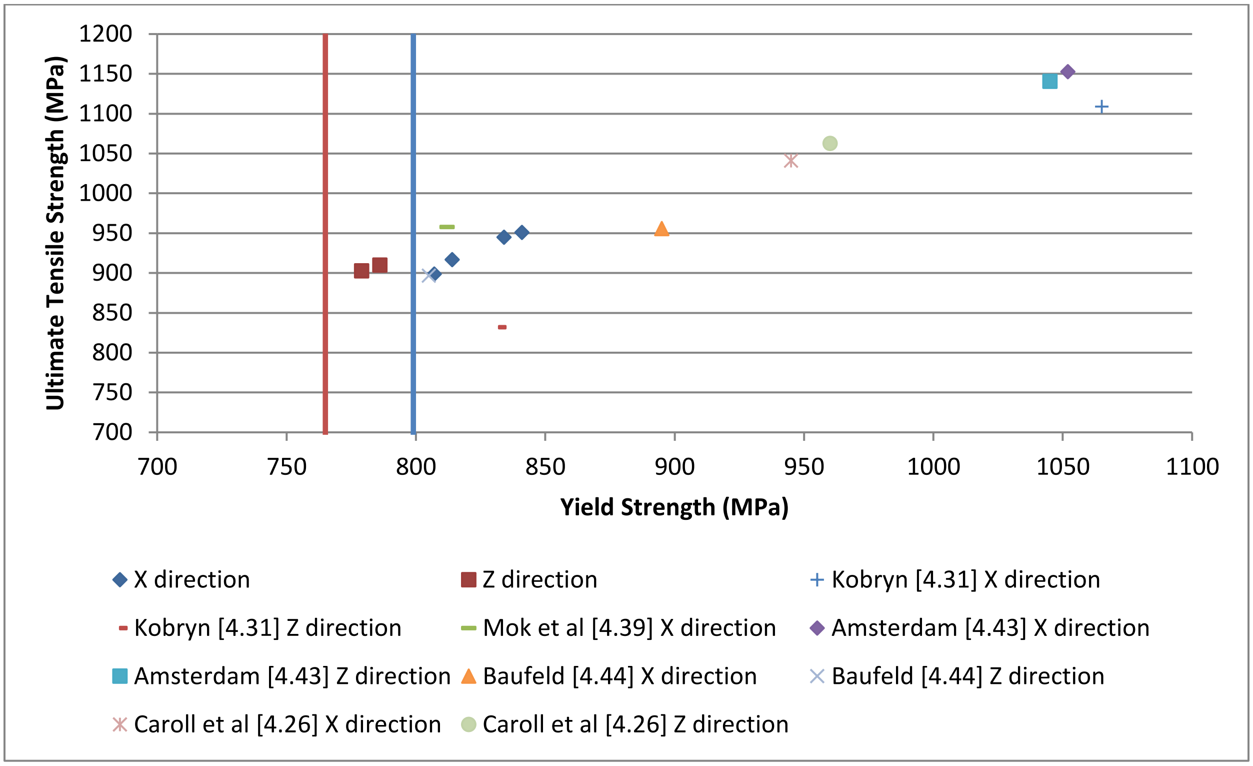


Figure 4-5: Ultimate Tensile Strength versus Yield Strength for DED stress relieved Ti-6Al-4V in the X and Z directions compared to existing values from the literature

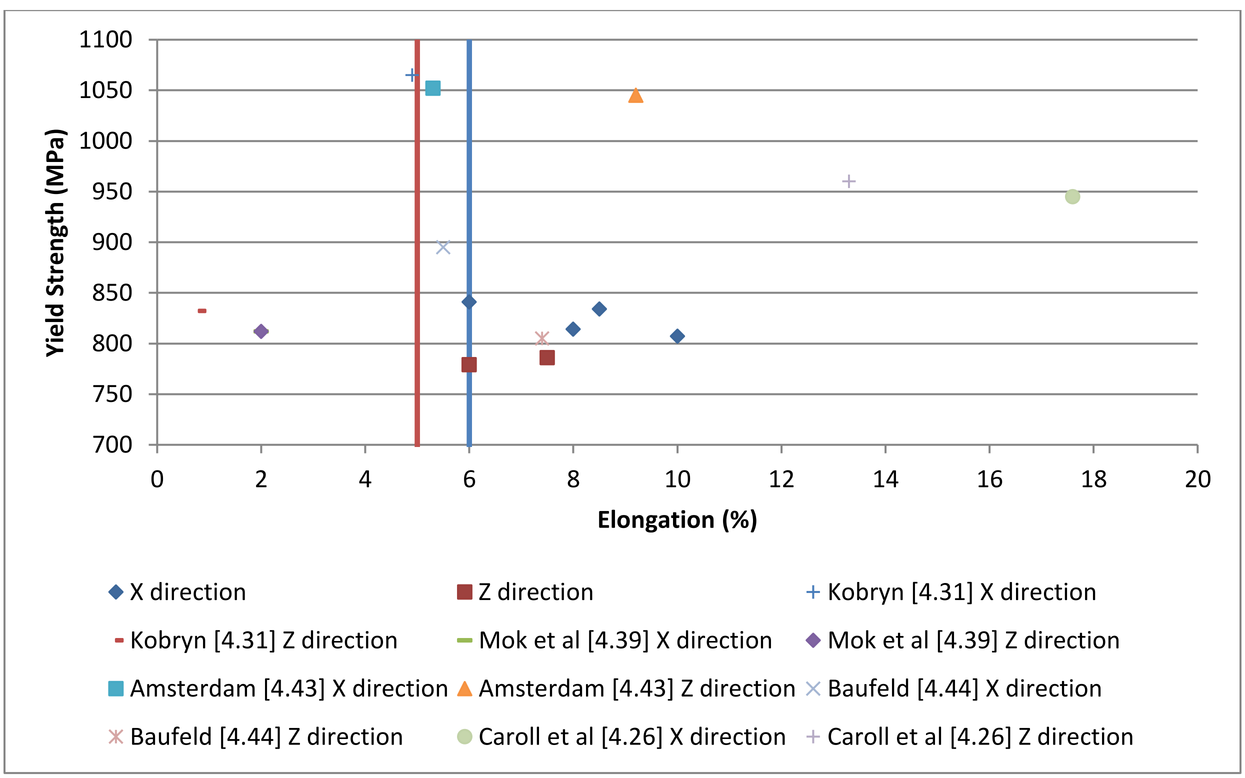


Figure 4-6: Yield Strength versus Final elongation for DED stress relieved Ti-6Al-4V in the X and Z directions compared to existing values from the literature

Figure 4-7: Broken tensile coupons; top: tested in the Z direction, bottom: tested in the X direction

As reported in the literature [4.11, 4.17, 4.26, 4.31, 4.39, 4.42, 4.43], the material tested in the X-direction (longitudinal) has slightly higher strength and lower ductility than in the Z-direction (transverse). Kobryn [4.31] attributed this anisotropy to the presence of lack-of-fusion pores. However, since the measured Young's modulus shows no direction dependence and is similar to the values reported for wrought or cast annealed Ti-6Al-4V [4.38], the anisotropic lack-of-fusion porosity can be excluded. In addition, the level of porosity in DED components is too small to have a significant impact on the properties. Baufeld et al. [4.27] suggested that the anisotropy is due to the presence of more grain boundaries along the X direction which is a potential cause for strengthening and provides preferential crack propagation paths reducing the elongation. For both directions of testing, the specimen size (gauge section diameter of 6 mm) and prior β grains size (405 ±120 µm) are comparable.

There will then be more numerous grain boundaries in the X direction, leading to a lower elongation [4.44]. Figure 4-7 shows the broken tensile coupons, exhibiting the ductile behavior of DED Ti-6Al-4V through necking [4.45]. There is a noticeable difference between the two directions of testing. In the X direction, the fracture surface show different failure planes exhibiting a mix between intergranular and transgranular fracture, when there is only one failure plane at 45° in the Z direction indicating a transgranular type of fracture. Further investigations of the fracture surfaces on both directions are shown on Figure 4-8. We can observe there the rupture plans for both directions. We can also notice that the main features on the fracture surface are round dimples.

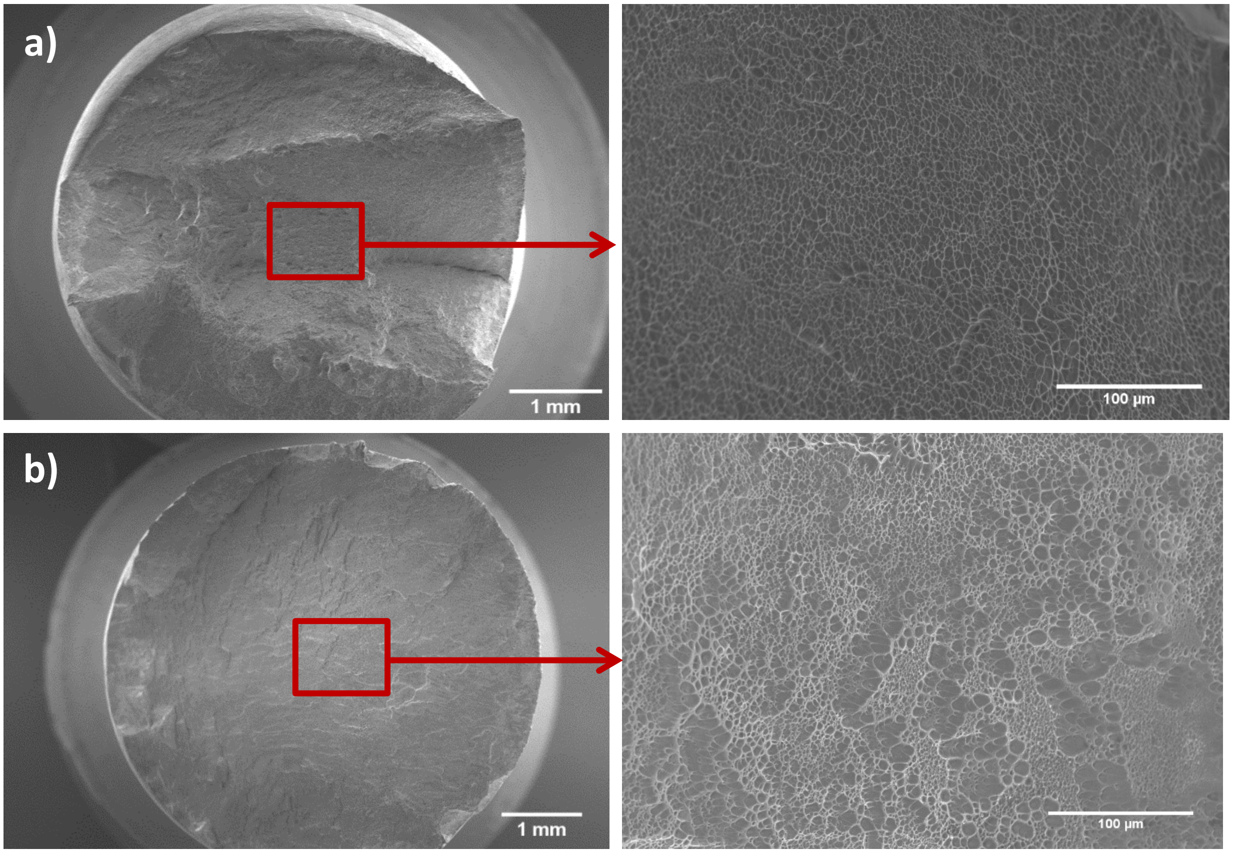

Figure 4-8: Fracture features of tensile coupons; a) X-direction, b) Z-direction

The dimples that appear on Figure 4-8 are another indication of the ductility of the material [4.46]. The elongation values for DED Ti-6Al-4V reported in the literature and shown on Figure 4-6 vary a lot. It was suggested that a finer microstructure would lead to increased ductility [4.27, 4.47], explaining the large range of final elongation found in the literature since the microstructure of DED components is affected by process parameters such as laser powder and cooling rate.

### 4.4.4 Fatigue Crack Growth

Fatigue Crack Growth Rate (FCGR) tests were conducted for three crack directions: parallel to the deposition direction (0°), perpendicular to the build direction (90°) and at 45° of the deposition direction. The three directions are shown on Figure 4-9, along with the plot of the Crack Growth Rate as a function of the stress Intensity factor. The data curve can be separated into three different regions: crack initiation near threshold ($\Delta K_{th}$), crack propagation under the Paris' Law ($\frac{da}{dn} = A\ \Delta K^{n}$) and instability leading to failure when the fracture toughness ($K_c$) is reached [4.48]. From curve fitting, data were obtained and given in Table 4-2 along with data for wrought or cast Ti-6Al-4V [4.38]. Similarly to previously published results [4.16, 4.49], there is no noticeable difference in the FCGR behavior between the three crack propagation directions. However, it can be noticed that the threshold and the fracture toughness are higher than those of wrought and cast Ti-6Al-4V. It has been reported that the crack path is not influenced by the boundaries of columnar β grains but by the presence and distribution of residual stress [4.16, 4.50]. In this work, the residual stresses induced by the thermal cycle of the process are removed by the stress relieve heat treatment, leading to an isotropic FCGR behavior.

Table 4-2: FCGR properties of as-built + stress relieved DED Ti-6Al-4V and wrought or cast Ti-6Al-4V

| Orientation | $\Delta K_{th}$ MPa √m | A In/cycle | n | $K_C$ MPa √m |
|---|---|---|---|---|
| 0° | 3 | $10^{-10}$ | 3.9 | 68 |
| 90° | 3 | $10^{-10}$ | 3.9 | 68 |
| 45° | 3.9 | $4 \times 10^{-10}$ | 3.5 | 70 |
| Wrought or cast alloy [4.38] | 10 to 20 | $10^{-10}$ | 3.9 | 50 to 80 |

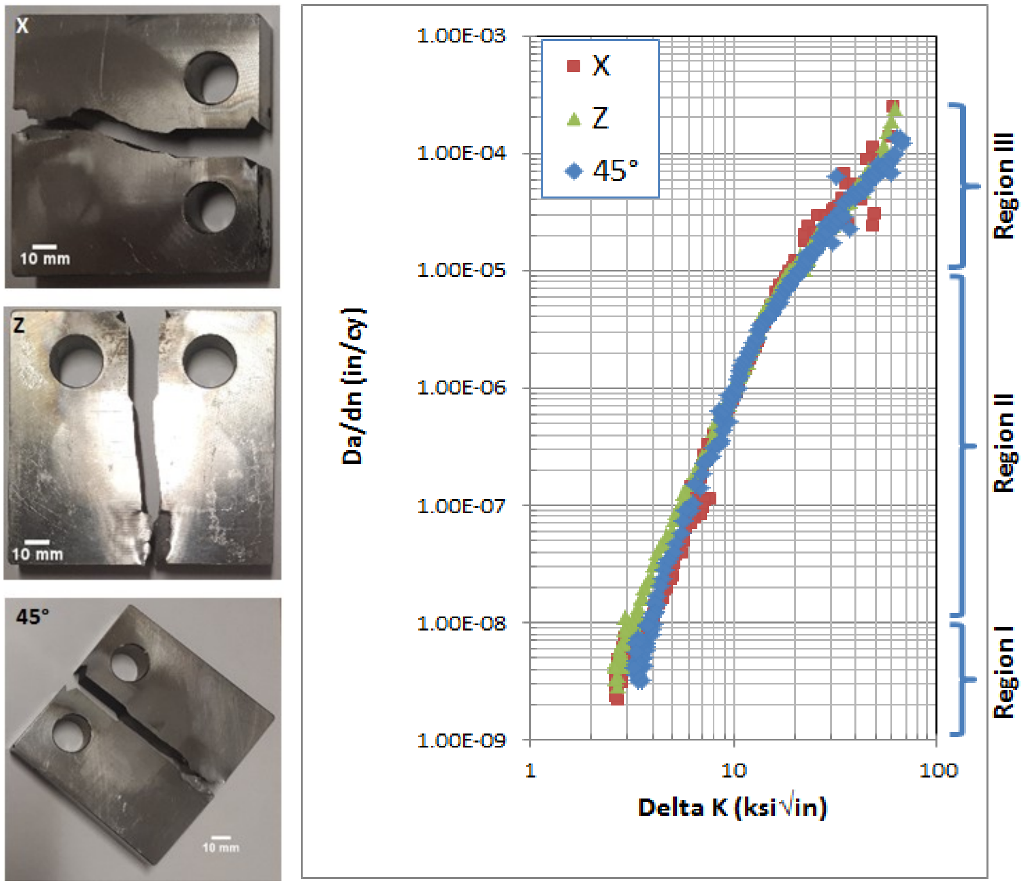


Figure 4-9: FCGR coupons and Crack Growth Rate versus Stress Intensity Factor for each direction

The fracture surface of the broken coupon with the crack propagating in the X direction is shows on Figure 4-10 and shows three areas corresponding to the three regions of the curve. The coupons with other crack propagation direction show the same three areas with the same features. Region I shows facets resulting from the crystallographic mode of crack propagation that happen near threshold and regions II shows fatigue features which appear in the form of terraces with dimples on top of them [4.51, 4.52]. Region III also show terrace-like features, but contrarily to those on region II, there have a rounder shape of 141 ±27 µm of diameter.

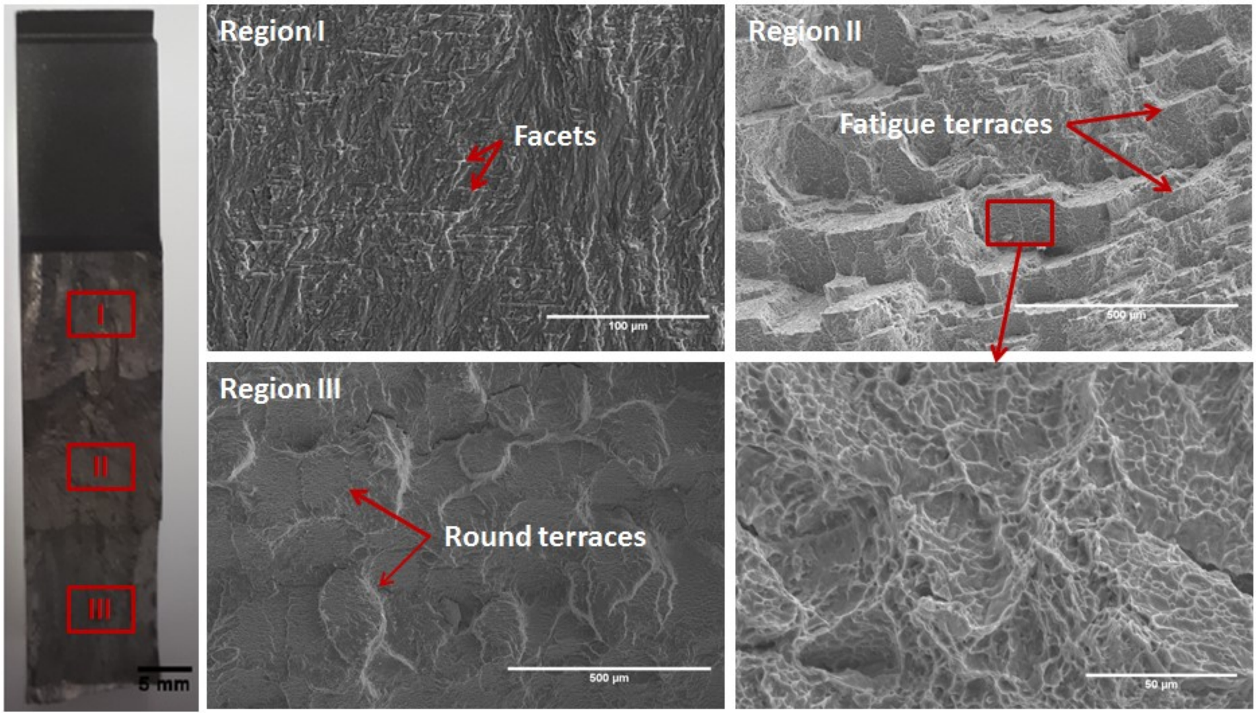


Figure 4-10: Fracture surfaces of FCGR coupon

Similar terraces-like structures have been observed in the literature where they are generally attributed to fracture in regions with a high level of porosity (around 0.1 %) [4.53, 4.54]. In this work, the level of porosity is around 0.12 % so the terraces are too numerous to be attributed to porosity. However, if the size of the round terraces is slightly smaller than the β grains size, those two features are of the same order magnitude, so it is possible that the terraces result from the crack propagation through prior β grains, as suggested by Simonelli et al. [4.50]. In region II, those structures are most probably the result of the repeated opening cycles.

### 4.4.5 Interface surface – build-up

As the parts were built on a Ti-6Al-4V wrought substrate, we extracted a coupon showing the interface between the substrate and the build-up part. Figure 4-11 shows the evolution of the microstructure from the substrate to the AM part. Three different areas define the interface: the top of the substrate, the Heat Affected Zone (HAZ) which is part of the substrate and was heated by the first layer of fused material, the Fusion Zone (FZ) which is part of the substrate and was heated by the first few layers of fused material [4.9, 4.55]. The substrate is a typical equiaxed structure [4.13] of both α and β phases which coarsen through the Heat Affected Zone to form prior β grains in the Fusion Zone that initiate the columnar growth observed in the AM part. Up to the third deposited layer with have an impact on the microstructure of the FZ and the HAZ [4.24]. Brandl et al. [4.9] described in details the influence of the deposition of the first layer on the substrate.

The substrate shows a bimodal microstructure made of globular primary α-grains in a basket weave α+β matrix. In the HAZ, two areas can be identified: $HAZ_{\beta}$ and $HAZ_{(\alpha+\beta)}$. $HAZ_{(\alpha+\beta)}$ is the zone heated to peak temperature below the β transus temperature. In the secondary $HAZ_{(\alpha+\beta)}$, there is a limited change compared to the base material. The lamella width of the basket-weave (α+β) matrix increased slightly and the grain size of the primary α-grains remained approximately constant. In the primary $HAZ_{(\alpha+\beta)}$, the basket-weave structure of the (α+β) matrix seems to change substantially to a colony structure, and the width of the α-lamellae seems to be finer. $HAZ_{\beta}$ is the zone heated to a peak temperature above the β transus temperature and below the solidus temperature. Here, the primary α-grains decreased in size or dissolved completely, and the prior β-grains increased in size slightly or substantially, depending on the peak temperature reached. The Fusion Zone (FZ) results from the solidification of the melt pool of the base material (for single bead or first deposited layer) or of the previously deposited layers (for multi-layers builds). The FZ and the build-up form a zone where the material is melted as the peak temperature exceeded the liquidus temperature. This zone is characterized by columnar prior β-grains with basket-weave structure and few martensitic α.


Figure 4-11: Microstructure and hardness profile of the interface substrate/build-up

On Figure 4-11, we can also observe the evolution of the hardness in the interface. In the first layers of the build-up, the hardness is similar to the one in the rest of the build-up reported earlier. In the substrate, the hardness is slightly smaller than the value provided by the manufacturer as the entire coupon undergoes a stress relief heat treatment. However, we can observe an increase of hardness in the FZ and the HAZ. In the HAZ, the hardness is increased as this zone underwent fast cooling leading to the formation of a non- equilibrium microstructure containing smaller α-lamella size and in the FZ, the cooling rate is further increased forming a basket-weave structure with a few martensitic α’ inducing further increase of the hardness [4.29]. This discontinuity in the hardness could expose a weakness in the repaired structure.

Further investigations are required to asset this weakness. A similar hardness profile was observed in the work of Yu et al. [4.56]

## 4.5 Summary

This work has investigated the properties of DED Ti-6Al-4V parts. In particular, the objective of the present research was to discuss the possibility of using DED as a repair process for aerospace components.

The microstructure developed in the build-up part is a Widmanstätten structure made of a mixture of α and β phases in prior β grains. Those columnar prior β grains induce anisotropy within the part. Regardless the direction of testing, the tensile properties of the as-build + stress relieved material fit the standard requirements and are very close to those of the wrought material. The FCGR tests suggest that the crack propagation is similar in the as-built and in the wrought material. Thus, the two materials are compatible for repair. The investigations on the interface suggest that the fusion and heat affected zones show a hardness mismatch that will make this region prone to failure and further work is necessary to evaluate and limit this risk of failure.

## 4.6 Acknowledgements

The authors would like to thank the CARIC, Liburdi, Héroux-Devtek Inc., Pratt & Whitney Canada, GNK Aerospace, Sheffield University, ECN and University of Ottawa for the financial and technical support of this research.

## 4.7 References

[1] B. Cantor, P. Grant, H. Assender, in *Aerospace Materials*, B. P. I. o. Physics, Ed., 2001.
[2] G. Lütjering and J.C. Williams, *Titanium (2nd Edition)*. Springer, 2007.

[3] D. Herzog, V. Seyda, E. Wycisk and C. Emmelmann, "Additive Manufacturing of Metals," *Acta Materialia,* vol. 117, pp. 371-392, 2016.
[4] E. Brandl, A. Schoberth, C. Leyens, "Morphology, microstructure, and hardness of titanium (Ti-6Al-4V) blocks deposited by wire-feed additive layer manufacturing (ALM)," *Materials Science and Engineering A,* vol. 532, pp. 295-307, 2012.
[5] T. Marazani, D.M. Madyira, E.T. Akinlabi, "Repair of cracks in metals: A review," *Procedia Manufacturing,* vol. 8, pp. 673-679, 2017.
[6] A.J. Pinkerton, W. Wang and L. Li, "Component repair using laser direct metal deposition," *Proc. IMechE, Part B: J. Engineering Manufacture,* vol. 222, 2007.
[7] B. Graf, A. Gumenyuk, M. Rethmeier, "Laser metal deposition as repair technology for stainless steel and titanium alloys " *Physics Procedia,* vol. 39, pp. 376-381, 2012.
[8] Nanda Kumar Dey, "Additive Manufacturing laser deposition of Ti-Al-4V for aerospace repair application," Masters, Missouri University of science and Technology, 2014.
[9] E. Brandl, V. Michailov, B. Viehweger and C. Leyens, "Deposition of Ti-6Al-4V using laser and wire, part I: Microstructural properties of single beads," *Surface & Coatings Technology,* vol. 206, pp. 1120-1129, 2011.
[10] E. Brandl, C. Leyens and F. Palm, "Mechanical Properties of Additive Manufactured Ti-6Al-4V Using Wire and Powder Based Processes," presented at the IOP Conf. Series: Materials Science and Engineering, 2011.
[11] B. Baufeld, "Effect of deposition parameters on mechanical properties of shaped metal deposition parts," *Proc. IMechE, Part B: J. Engineering Manufacture,* vol. 226, pp. 126-136, 2012.
[12] J. Gockel et al., "Trends in solidification grain size and morphology for additive manufacturing of Ti-6Al-4V," *JOM,* vol. 69, no. 12, pp. 2706-2710, 2017.
[13] D.A. Porter, K.E. Easterling, M.Y. Sherif, *Phase Transformations in Metals and Alloys, Third Edition*. CRC Press, 2009.
[14] B. Baufeld, O. Van der Biest and R. Gault, "Additive manufacturing of Ti-6Al-4V components by shaped metal deposition: Microstructure and mechanical properties," *Materials and Design,* vol. 31, pp. 5106-5111, 2010.
[15] S.A. David and J.M. Vitek, "Correlation between solidification parameters and weld microstructure," *International Materials Reviews,* vol. 34, no. 5, pp. 213-245, 1989.
[16] R. Konecna, L. Kunz, A. Baca and G. Nicoletto, "Long fatigue crack growth in Ti6Al4V produced by direct metal laser sintering," *Procedia Engineering,* vol. 160, no. 69-76, 2016.
[17] J.J. Lewandowski and M. Seifi, "Metal Additive Manufacturing: A review of Mechanical properties," *Annual Review of Materials Research,* vol. 46, no. 151-186, 2016.
[18] A.J. Streling, B. Torries, N. Shamsaei, S.M. Thompson and D.W. Seely, "Fatigue behavior and failure mechanisms of direct laser deposited Ti–6Al–4V," *Materials Science & Engineering A,* vol. 655, pp. 100-112, 2016.
[19] B. Rottwinkel, C. Nölke, S. Kaierle, V. Wesling, "Crack repair of single crystal turbine blades using laser cladding technology," *Procedia CIRP,* vol. 22, pp. 263-267, 2014.
[20] *ASM2801B: Heat Treatment of Titanium Alloy Parts*, 2014.
[21] *ASTM E112: Standard Test Methods for Determining Average Grain Size*, 2013.
[22] *ASTM E8/E8M: Standard Test Method for Tension Testing of Metallic Materials*, 2016.

[23] *ASTM E647: Standard Test Method for Measurements of Fatigue Crack Growth Rates*, 2015.

[24] S.M. Kelly and S.L. Kampe, "Microstructural Evolution in Laser-Deposited Multilayer Ti-6Al-4V Builds: Part I. Microstructural Characterization," *Metallurgical and Materials Transactions A,* vol. 35, pp. 1861-1867, 2004.

[25] G.P. Dinda, L. Song, J. Mazumder, "Fabrication of Ti-6Al-4V Scaffolds by Direct Metal Deposition," *Metallurgical and Materials Transactions A,* vol. 39, pp. 2914-2922, 2008.

[26] B.E. Caroll, T.A. Palmer and A.M. Beese, "Anisotropic tensile behavior of Ti-6Al-4V components fabricated with direct energy deposition additive manufacturing," *Acta Materialia,* vol. 87, pp. 309-320, 2015.

[27] B. Baufeld, E. Brandl and O. Van der Biest, "Wire based additive layer manufacturing: Comparison of microstructure and mechanical properties of Ti-6Al-4V components fabricated by laser-beam deposition and shaped metal deposition," *Journal of Materials Processing Technology,* vol. 211, pp. 1146-1158, 2011.

[28] C. Charles and N. Järvstrat, "Modelling Ti–6Al–4V microstructure by evolution laws implemented as finite element subroutines: application to TIG metal deposition," presented at the 8th International conference on trends in welding research, Pine Mountain, GA, USA, 2008.

[29] E. Brandl, V. Michailov, B. Viehweger and C. Leyens, "Deposition of Ti-6Al-4V using laser and wire, part II: Hardness and dimensions of single beads," *Surface & Coatings Technology,* vol. 206, pp. 1130-1141, 2011.

[30] J. Alcisto et al., "Tensile Properties and Microstructures of Laser-Formed Ti-6Al-4V," *Journal of Materials Engineering and Performance,* vol. 20, pp. 203-212, 2011.

[31] P.A. Kobryn and S.L. Semiatin, "Mechanical Properties of Laser-Deposited Ti-6Al-4V," *AFRL/MLLMP,* pp. 179-186, 2002.

[32] S.L. Semiatin, S.L. Knisley, P.N. Fagin, F. Zhang and D.R. Barker "Microstructure and texture evolution during solidification processing of Ti–6Al–4V," *Journal of Materials Processing Technology,,* vol. 135, pp. 330-339, 2003.

[33] S.M. Kelly and S.L. Kampe, "Microstructural evolution in laser-deposited multilayer Ti–6Al–4V builds: Part II. Thermal modeling," *Metallurgical and Materials Transactions A,* vol. 35, pp. 1869-1879, 2004.

[34] J. Irwin, E.W. eutzel, P. Michaleris, J. Keist and A.R. Nassar, "Predicting Microstructure form Thermal History during Additive Manufacturing for Ti-6Al-4V," *Journal of Materials Science and Engineering,* vol. 138, no. 11, pp. 138-149, 2016.

[35] C. Qiu et al., "Fabrication of large Ti-6Al-4V structures by direct laser deposition," *Alloys and Compounds,* vol. 619, pp. 351-361, 2015.

[36] S. J. Wolff et al., "A framework to link localized cooling and properties of directed energy deposition (DED)-processed Ti-6Al-4V," *Acta Materialia,* vol. 132, pp. 106-117, 2017.

[37] P.A. Kobryn, E.H. Moore and S.L. Semiatin, "The effect of Laser Power and Transverse speed on Microstructure, Porosity, and Build Height in Laser-Deposited Ti-6Al-4V," *Scripta mater.,* vol. 43, pp. 299-305, 2000.

[38] R. Boyer, G. Welsch and E.W. Collings, *Materials Properties Handbook: Titanium Alloys*. ASM International, 1994.

[39] S.H. Mok et al., "Deposition of Ti-6Al-4V using a high power diode laser and wire, part II: Investigation on the mechanical properties," *Surface & Coatings Technology,* vol. 202, pp. 4613-4619, 2008.

[40] X. Tan, Y. Kok, Y.J. Tan, M. Descoins, D. Mangelinck, S.B. Tor, K.F Leong, C.K. Chua, "Graded microstructure and mechanical properties of additive manufactured Ti–6Al–4V via electron beam melting," *Acta Materialia,* vol. 97, pp. 1-16, 2015.

[41] *AMS4999A: Titanium Alloy Direct Deposited Product 6Al-4V Annealed*, 2011.

[42] E. Brandl, F. Palm, V. Michailov, V. Viehweger, C. Leyens, "Mechanical properties of additive manufactured titanium (Ti-6Al-4V) blocks deposited by a solid-state laser and wire," *Materials and Design,* vol. 32, pp. 4665-4675, 2011.

[43] E. Amsterdam and G.A. Kool, "High cycle fatigue of laser beam deposited Ti-6Al-4V and Inconel 718," presented at the 25th ICAF Symposium: Bridging the Gap between Theory and Operational Practice, 2009.

[44] B. Baufeld and O. Van der Biest, "Mechanical properties of Ti-6Al-4V specimens produced by shaped metal deposition," *Science and Technology of Advanced Materials,* vol. 10, 2009.

[45] W.D. Callister Jr, *Fundamentals of materials science and engineering, 5th ed*. John Wiley & Sons, 2001.

[46] V.A. Joshi, *Titanium alloys: an atlas of structures and fracture features*. CRC Press, 2006.

[47] W. Xu, M. Brandt, S. Sun, J. Elambasseril, Q. Liu, K. Lathma, K. Xia and M. Qian, "Additive Manufacturing of strong and ductile Ti-6Al-4V by selective laser melting via in situ martensite decomposition," *Acta Materialia,* vol. 85, pp. 74-84, 2015.

[48] R.I. Stephens and H.O. Fuchs, "Metal Fatigue in Engineering," New York: Wiley, 2001.

[49] V. Cain, L. Thijs, J. Van Humbeeck, B. Van Hooreweder and R. Knutsen, "Crack propagation and fracture toughness of Ti6Al4V alloy produced by selective laser melting," *Additive Manufacturing,* vol. 5, pp. 68-76, 2015.

[50] M. Simmonelli, Y.Y. Tse and C. Tuck, "Effect of the build orientation on the mechanical properties and the fracture modes of SLM Ti-6AL-4V," *Materials Science & Engineering A,* vol. 616, pp. 1-11, 2014.

[51] C. Bathias, K. El Alami and T.Y. Wu, "Influence of mean stress on Ti6Al4V fatigue crack growth at very high frequency," *Engineering Fracture Mechanics,* vol. 56, pp. 255-264, 1997.

[52] Y. Zhai, H. Galarraga and D.A. Lados, "Microstructure, static properties, and fatigue crack growth mechanisms in Ti-6Al-4V fabricated by additive manufacturing: LENS and EBM," *Engineering Failure Analysis,* vol. 69, pp. 3-14, 2016.

[53] C. Qiu, N.J.E. Adkins, M.M. Attalah, "Microstructure and tensile properties of selectively laser-melted and of HIPed laser-melted Ti–6Al–4V," *Materials Science & Engineering A,* vol. 578, pp. 230-239, 2013.

[54] T. Vilaro, C. Colin and J.D. Bartout, "As-Fabricated and Heat-Treated Microstructures of the Ti-6Al-4V Alloy Processed by Selective Laser Melting," *Metallurgical and Materials Transactions A,* vol. 42, pp. 3190-3199, 2011.

[55] S. Kou, *Welding Metallurgy, Second Edition*. John Wiley & Sons Inc, 2003.

[56] J. Yu, M. Rombouts, G. Maes and F. Motmans, "Materials properties of Ti-6Al-4V parts produced by laser metal deposition," *Physics Procedia,* vol. 39, pp. 416-424, 2012.

# Chapitre 5 - Summary

This objective of this work was to investigate the characteristics of DED Ti-6Al-4V in a context of repair. Coupons were produced throughout the deposition of Ti-6Al-4V wire spool with Extra-Low Interstitials on rolled annealed grade 5 Ti-6Al-4V substrates using a Yb:YAG fiber laser in an argon atmosphere. Characterization campaigns led to assessment of the microstructure, hardness, tensile behavior and fatigue crack growth resistance of the deposited material. This chapter provides a summary of the work realized during this project.

- The DED process yielded the formation of columnar prior β grains along the build direction. A Widmanstätten structure made of a mixture of α and β phases developed inside these transformed grains. The microstructure of each layer is influenced by the thermal cycle imposed by the three following layers, leading to the observation of microstructure gradient in the part.
- The hardness measurements indicated that DED has lower strength than wrought annealed Ti-6Al-4V.
- The tensile behavior of the DED material exhibits some anisotropy. The X-direction shows higher strength and lower ductility than the Z-direction. All coupons tested in this work meet the AMS 4999A standard requirements for DED Ti-6Al-4V.
- The FCGR behavior in the Paris' law region is similar for the one for wrought and cast Ti-6Al-4V, even though the threshold value indicated that a crack propagate more easily in the DED material, which however has increased fatigue life.
- The evolution of the microstructure at the repaired interface necessary to go from and equiaxed microstructure of the substrate to the columnar grains of the DED parts creates a step in the hardness profile that suggests a reduction in the mechanical properties of the interface.